Department of Precision and Microsystems Engineering

Mechanical design for out-of-plane mode attenuation in flexure mechanisms

Giovanni Marega

Report no : 2022.042
Coach : M.B. Kaczmarek
Professor : Dr. S.H. HosseinNia
Specialisation : Mechatronic System Design
Type of report : Master Thesis
Date : 15 August 2022

Mechanical design for out-of-plane mode attenuation in flexure mechanisms

by

Giovanni Marega

Student number: 5377641

Thesis committee:	Dr. ir. S.H. HosseinNia,	TU Delft, supervisor
	Marcin Kaczmarek	TU Delft, supervisor
	Prof.dr. P.G. Steeneken,	TU Delft

TU Delft

Preface

This thesis represents the end of my studies at the TU Delft. It has been a great experience and I would like to thank the people that helped me during the project, which took an entire academic year.

First, I would like to thank my supervisor Marcin for his continuous presence and help. Your indications have really helped to get through the most difficult stages of the thesis. Then, I would also like to thank Hassan for his support, especially in the final part of the project. I really appreciated the fact that both of you gave me the possibility to work on an open topic, instead of restricting my options of research.

Finally, I would like to thank the other students in the MSD Group. We had the possibility to share our ideas and opinions on a weekly basis and this was not only useful but also stimulating. I really enjoyed our meetings and I would like to thank you again for your time and support.

Giovanni Marega
Delft, August 2022

Summary

The problem of vibrations in the high-tech industry is becoming increasingly important. Indeed, the applications of compliant flexible mechanism over classical rigid ones are rising since they offer many advantages. Furthermore, machines are pushed to move faster to increase the productivity. Therefore, flexible systems are operated at high frequencies and unwanted vibrations are generated. In particular, the most problematic vibrations in machines involving compliant flexure mechanisms are represented by flexural modes, i.e. by vibrations that occur in the most compliant direction of the mechanism. However, also out-of-plane modes, that occur in the space outside the nominal plane of movement of the mechanism, can be very important, especially in machines with several and coupled degrees of freedom, like 3D positioning stages.

The literature about vibration control for flexural modes is very rich. However, the problem represented by out-of-plane modes is scarcely covered. The solutions that are proposed so far for out-of-plane mode attenuation do not look convincing and the possibility to use other vibration control methods still has to be explored.

Therefore, in this work two new design solutions, one involving piezoelectric materials and the other Eddy current dampers (ECDs), are proposed to achieve out-of-plane mode attenuation in flexure mechanisms. Such damping methods are chosen because of their attractive properties. On the one hand, piezoelectric materials represent the spearhead in the class of the so-called ”smart materials”, which are materials able to connect different physical domains, and are shown to be able to provide effective vibration attenuation in flexible systems. On the other hand, ECDs are based on magnets, which are very common in the high-tech industry: moreover, they are reliable, thermally stable, can be applied in vacuum and do not rely on mechanical contact.

Overall, it is shown that the strategy based on ECD for out-of-plane mode attenuation is not suitable, differently from the one based on the piezoelectric effect. The effectiveness of such technique is validated both analytically and using a FEM software. In particular, the analytical model is based on Hamilton’s principle, Rayleigh-Ritz procedure and Euler-Bernoulli beam theory, while $COMSOL\ Multiphysics$ is used to numerically validate the design.

Contents

1 Introduction

1.1. Motivation and problem definition

The high-tech applications of compliant mechanisms over classical rigid ones are continuously increasing over the last decades. Indeed, they offer many advantages such as very low friction, no backlash, no need of lubrication and compactness [1]. However, they are susceptible to vibrations because of their flexible nature and this drawback is very relevant in the industry. In fact, in the high-tech field there is strive to increase both the productivity and the quality of products. In other words, machines are pushed to be more precise and to operate at higher frequencies at the same time. As a consequence, compliant flexible mechanisms are pushed to move faster and faster, leading to undesired vibrations, which in turn cause a reduction in the accuracy and in the lifetime of machines.

Therefore, the study on possible solutions to attenuate vibrations in compliant mechanisms is of interest. However, before starting to think about solutions, it is necessary to understand the nature of such vibrations. The most relevant and problematic mode of vibration in compliant flexure mechanisms is the so-called ”flexural” mode, which takes place in the most compliant direction of the flexure, which is generally the direction in which the flexure and the machine are supposed to move. The other types of mode that can occur in flexure mechanisms, which can be either translational or rotational, typically consist in a deflection in a direction perpendicular to the one where the more common flexural modes occur. In other words, these less familiar modes of vibration take place perpendicularly with respect to the desired direction or plane of movement of the mechanism: for this reason, they can be classified as ”out-of-plane” modes. An example of flexural and out-of-plane modes is illustrated in Figure 1.1.

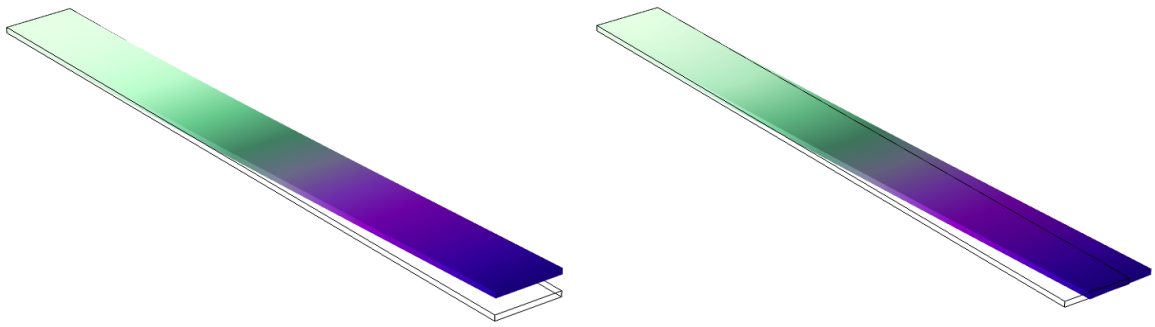

(a) Flexural mode

(b) Out-of-plane mode

Figure 1.1

There exist plenty of techniques to tackle vibrations in flexure systems and they are typically applied to flexural modes. The problem of out-of-plane modes is generally underestimated, since they occur at

higher frequencies and they are more difficult to excite. However, also such kind of vibrations can be relevant, especially in complex mechanisms with coupled degrees of freedom, such as 3D positioning stages. An example of such kind of mechanism is given in Figure 1.2, where piezoelectric actuators are employed to move the machine. For instance, it can be observed that if the z-axis piezo is actuated, it excites both the x-axis and the y-axis stages in their out-of-plane direction, which is the z-direction. Therefore, if the z-axis piezo is operated in the vicinity of one of the out-of-plane eigenfrequencies for either the x-axis or the y-axis stage, undesired out-of-plane deflections may arise. Therefore, this work is focused on the less explored problem of out-of-plane vibration attenuation in flexure mechanisms.

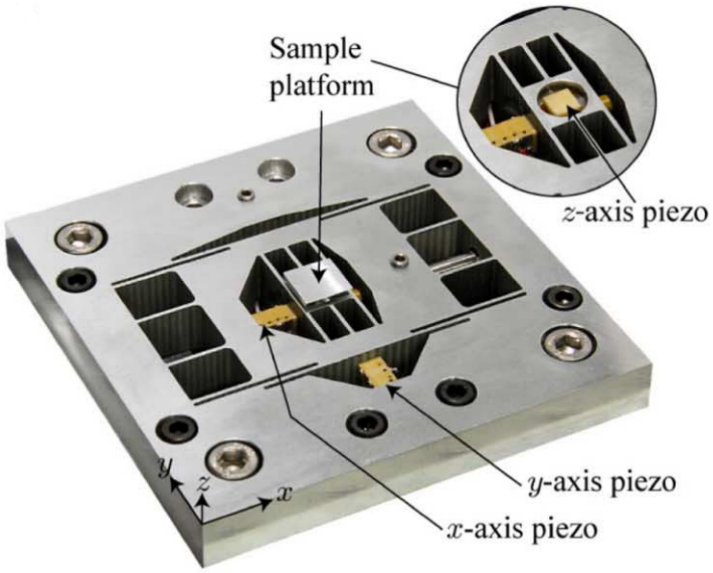

Figure 1.2: 3D positioning stage [2]

1.2. Prior art

As just mentioned, the literature on out-of-plane vibration attenuation in flexure mechanisms is quite scarce since such kind of mode is typically more difficult to excite than the flexural one. Nevertheless, some solutions are already present. In the mechanisms of the aformentioned Figure 1.2, the strategy consists in designing the stage geometry and the flexure configuration such that the out-of-plane stiffness-to mass ratios are higher than the actuation stiffness-to-mass ratio [2]. This solution is effective but it does not really solve the problem of out-of-plane vibrations, it avoids it. Indeed, this solution is based on the idea that optimizing the geometry of the mechanism it is possible to have the actuation modes, i.e. the flexural modes, occurring before the out-of-plane ones, avoiding the problem of out-of-plane deformations. Therefore, if the mechanism somehow undergoes out-of-plane vibrations, because of external forces, disturbances or design errors, there is not a designed solution able to attenuate them.

Furthermore, there is the possibility to increase the out-of-plane stiffness in flexure mechanisms by adding compliant bearings able to allow to movement in the nominal directions of motion and further constrain it in the out-of-plane direction. This principle can be appreciated in Figure 1.3, which represents an XY positioning stage. The added elements do not interfere with the motion in the XY plane and strongly increase the out-of-plane stiffness and payload capacity of the mechanism. This method could be applied also for the attenuation of stiff out-of-plane modes. However, it is cumbersome, it adds a non-negligible amount of weight, it increases the manufacturing complexity and it strongly increases the stiffness in the nominal directions of motion.

Finally, viscoelastic materials such as foams could be attached to flexures [4], as represented in Figure 1.4. In such mechanism, the foams help to attenuate any kind of vibrations, including out-of-plane modes. The vibrational energy is converted into heat thanks to the hysteresis that characterizes the

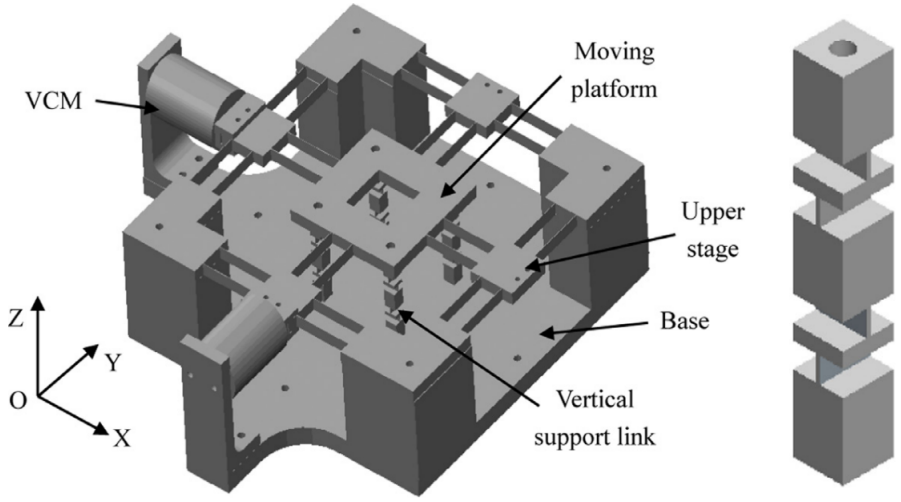

Figure 1.3: 2D positioning stage with increased out-of-plane load capacity [3]

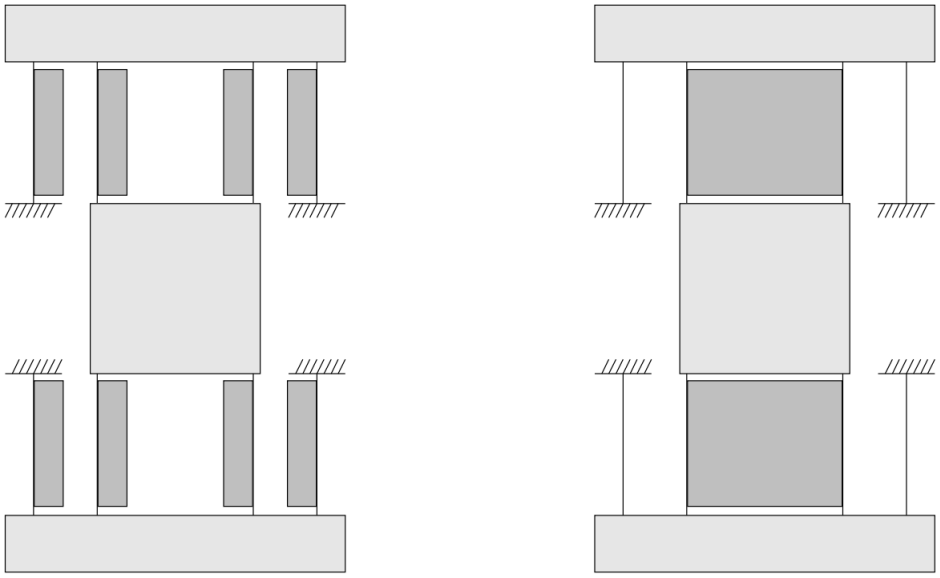

Figure 1.4: Flexure mechanism with foams for out-of-plane vibration attenuation [4]

loading and unloading curves of viscoelastic materials, giving rise to a damping effect. This technique is effective because viscoelastic damping is suitable at high frequencies, where stiff modes, i.e. out-of-plane modes, are to be found. However, such kind of material is strongly temperature and frequency dependent. Moreover, it out-gasses and as a consequence cannot be applied in vacuum.

1.3. Research goal and structure of the thesis

The previous work on out-of-plane vibration attenuation is not extensive. Therefore, new methods to tackle such problem would be helpful. The research goal of this work is to find and validate alternative solutions with respect to the ones found in the literature.

In particular, two new possible vibration control strategies could be employed: piezoelectric shunt damping and Eddy current damping. These two damping techniques are selected for multiple reasons. The main reason is that they both can provide effective damping in a passive way, i.e. without the aid of any external energy or control algorithm: out-of-plane eigenfrequencies are typically very high and at high frequencies passive solutions are preferred over active ones. In fact, active vibration control

strategies, which rely on external power supplies and controllers, may be affected by bandwidth limitations of the actuators and spillover effects, i.e. unexpected higher order modes may deteriorate the damping performances. Furthermore, piezoelectric materials are ”smart materials”, able to couple two different physical domains, while Eddy current dampers can give rise to very elegant solutions since they are not based on mechanical contact.

Therefore, after directing the research towards such damping techniques, new designs for out-of-plane mode attenuation are developed. However, before introducing the design concepts, in chapter 2 the background knowledge on piezoelectricity and Eddy currents is illustrated. Then, in chapter 3 the piezoelectric-based design will be outlined and its effectiveness validated. Furthermore, in chapter 4, the ECD-based solution is illustrated and shown to be not suitable for out-of-plane mode attenuation. Finally, in chapter 5 the thesis is concluded and recommendations for future work are provided.

2

Preliminary: piezoelectric-based damping and Eddy current damping

In this chapter, general background knowledge about piezoelectric-based damping and Eddy current damping is introduced. If the reader is familiar with such fields of science, it is possible to skip this discussion and go directly to the chapters on the new designs for out-of-plane mode attenuation, i.e. chapter 3 and chapter 4.

2.1. Piezoelectric-based damping

The emergence of the so-called smart materials over the last decades is leading to new solutions in the field of vibration attenuation. These special materials have the ability to respond significantly to stimuli of different physical natures [5].

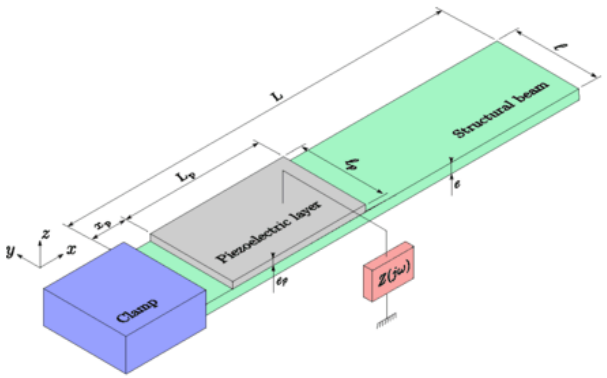

Figure 2.1: Schematic of a smart piezoelectric-shunted beam [6]

Among the smart materials of practical interest, piezoelectric materials are the most used. In fact, these materials can be used for both sensing, relying on the direct piezoelectric effect, and actuation, using the inverse piezoelectric effect [7].

Piezoelectricity is the phenomenon that characterizes materials that originate electric charges once they are deformed (direct pizoelectric effect) and that, viceversa, give rise to changes to their dimensions as they are subjected to external electric fields (inverse piezoelectric effect).

Piezoelectric materials can be used as strain sensors when they are mechanically bonded to a deforming structure and rely on the direct piezoelectric effect. Indeed, the deformation occurs also for the piezoelectric material, giving rise to electric charges on its surfaces, whose amount can be linearly related to the amount of deformation. On the contrary, the piezoelectric actuators are based on the

inverse piezoelectric effect [5].

Piezoelectric materials can be effectively used both in a passive and in an active way in the field of vibration control. In the next two paragraphs, the passive technique, i.e. the so-called ”piezoelectric shunt damping”, and the active one are outlined.

2.1.1. Piezoelectric shunt damping

The most common passive control method involving piezoelectric materials is represented by the so-called piezoelectric shunt damping, which is schematically illustrated in Figure 2.1. This technique consists in connecting electric or electronic circuits (indicated by impedance $Z(\omega)$ in Figure 2.1) to the electrodes of a piezoelectric transducer bonded to a vibrating structure [6], defined also as ”smart” structure because of the presence of the ”smart” piezoelectric material. In this way, the mechanical vibrations cause the piezoelectric material to generate electric charges according to the direct piezoelectric effect and these charges generate in turn an electric current in the circuit, composed by the piezoelectric transducer (which can be seen as a capacitor) and by the shunt impedance $Z(\omega)$. Therefore, the mechanical vibrational energy is converted, partially, into electric energy which is then dissipated in the circuit with a proper selection of the impedance $Z(\omega)$.

The characteristics of the electric circuit, the material properties and the dimensions and positions of the piezoelectric elements determine the effectiveness of the damping action. As a general guideline, in the case of flexible structures such as cantilever beams, the piezoelectric patches should be placed at the locations of maximum modal strain energy [8]. For example, in Figure 2.1 it can be seen that the piezo is placed next to the clamp, which is where the maximum strain can be observed as the beam bends downwards at the first eigenfrequency.

Many kinds of electric shunt circuits are proposed and studied, some of them are simple and give the possibility to dampen only one mode, while others are more complex and can dampen several modes: for a detailed illustration of the possible shunt circuits, the reader is referred to the review of [9]. One of the most studied ones is the series RL-shunt circuit: if the electrical eigenfrequency is properly tuned, it leads to an effective means of achieving vibration attenuation. Indeed, given the inherent capacitance of the piezoelectric transducer, C_p, the two other parameters of the resonant circuit can be tuned with respect to a particular natural frequency of the mechanical structure for achieving minimum vibration amplitudes in the vicinity of that frequency. The formulae for determining the optimal values L_{opt} and R_{opt} for the RL-shunt circuit are [10]:

$$R_{opt} = \sqrt{2}\frac{K_i}{(1 + {K_i}^2)C_p\omega_n} \tag{2.1}$$

$$L_{opt} = \frac{1}{(1 + {K_i}^2)C_p{\omega_n}^2} \tag{2.2}$$

where ω_n is a normalization frequency, chosen typically very close to the structural eigenfrequency, C_p is the electric capacitance of the piezoelectric transducer and K_i is the electromechanical coupling coefficient, which can be identified from experimentally measured open-circuit and short-circuit natural frequencies but also estimated analytically, as for example in [11].

It is worth noticing that the value for the inductance has to be generally high. Therefore, instead of using real and bulky inductors, synthetic inductors that rely on operational amplifiers are often preferred [12]. Then, the piezoelectric shunt is said to be semi-passive, since such electronic devices are active but they are used to create a circuit that behaves like a passive one.

Referring to the system of Figure 2.1, it can be demonstrated that the vibration amplitude of the tip of the cantilever beam varies with the frequency of excitation following the curves plotted in figure Figure 2.2. Therefore, it can be observed that the system becomes very similar to the one with a tuned mass damper if the shunt impedance has an inductance, since two resonance peaks are present.

Furthermore, it can also be noticed that a proper selection of the components in the shunt is essential to achieve high vibration attenuation.

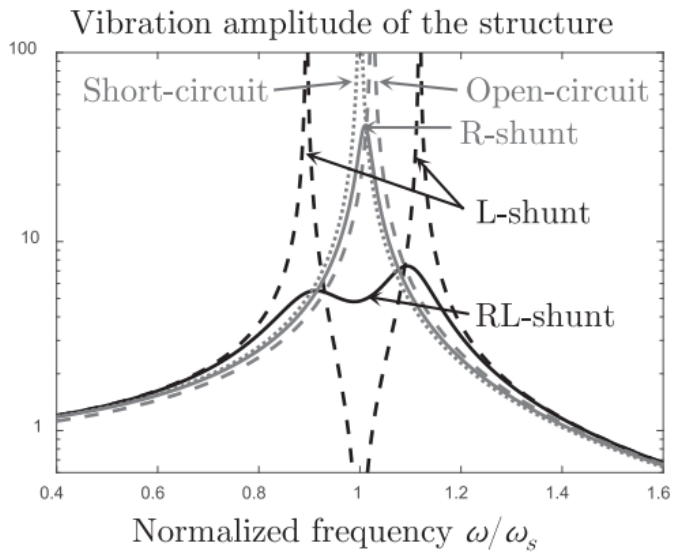

Figure 2.2: Typical frequency response function of a shunted piezoelectric material bonded to a vibrating structure [9]

Furthermore, it can be observed that the inherent capacitance C_p of the piezo represents an obstacle for the dissipation of the electric energy, since it represents a negative impedance, equal to $\frac{-j}{\omega C}$. Indeed, the RL shunt can effectively damp eigenmodes since the negative impedance that characterizes the capacitance C_p is compensated by the positive impedance of the inductance L, equal to $j\omega L$ in correspondence of the electrical eigenfrequency. However, this compensation occurs only at the eigenfrequency, therefore synthetic negative capacitance circuits, made using OpAmps, are often used to eliminate the capacitive behavior of the shunt [13]. This solution, however, carries the risk of instability.

Moreover, as already mentioned, the effectiveness of piezoelectric shunt damping strongly decreases if the electric impedance is not tuned properly. Therefore, adaptive shunt circuits, which are able to perform online adaptation of their impedance, are proposed and created in order to solve the detuning problem [14]. Even though this solution can give satisfactory results, its implementation is complex and requires plenty of electronic components.

Finally, another damping technique based on piezoelectric materials is the so-called synchronized-switch-damping (SSD). This technique consists in inverting repeatedly the voltage on the piezo synchronously with the structural motion in order to change its stiffness in a convenient manner [15]. Therefore, this technique is suitable for multimode damping, since the frequency at which the voltage is inverted can be obviously varied. More specifically, the basic principle of SSD consists in the fact that the piezoelectric material is used to dampen when needed only: therefore, if the structure moves away from the equilibrium position, the transducer is allowed to damp (i.e. set to ”high stiffness state”) otherwise it is not (”low stiffness state”). This technique is effective but it requires full state feedback and is not suitable for high frequencies due to phase lags [16]. Indeed, the effectiveness of this method is based on the fact that the piezos change their stiffness at the right moment and delays in the switching can degrade drastically the performance.

Overall, piezoelectric shunt damping represent a new and very interesting field of research, since it represents a lightweight and effective solution to attenuate vibrations in flexible systems and its limitations, such as the detuning problem of the shunt impedance, can be circumvented.

2.1.2. Piezoelectric active vibration control

Active damping, also defined as active vibration control (AVC), typically consists in driving actuators used to damp structures relying on power supplies, sensors and controllers. Active vibration control can be performed in different ways, using for example piezoelectric materials [5] or electromagnets [17]. AVC strategies are known for their high damping performances when compared to passive methods, but they can be employed only at relatively low frequencies because of bandwidth limitations. The most studied AVC technique is represented by active piezoelectric materials. Indeed, as already outlined in the section for piezoelectric shunt damping, piezoelectric transducers offer many advantages and are characterized by excellent repeatability, small hysteresis, stability, high stiffness, ease of integration, low cost, vacuum-proof and they are usable in a wide-frequency operation range [5]. Furthermore, they are generally very effective, especially at low frequencies, when compared to passive techniques. For example, it is demonstrated that for a certain configuration of piezoelectric patches attached to a cantilever beam, if the piezoelectrics are passively shunted the eigenmode attenuation is about 14 dB, while with active control is goes up to 28 dB [18]. A simplified schematic of piezoelectric AVC of a beam is shown in Figure 2.3.

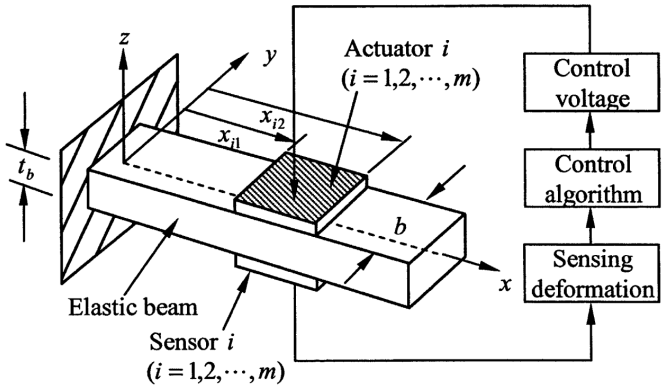

Figure 2.3: Typical AVC layout based on piezoelectric components [19]

In the following sections, the focus is set on the mathematical formulation of the piezoelectric effect.

Actuation

The constitutive equations describing piezoelectric materials, i.e. the piezoelectric effect, are [5]:

$$S_{ij} = s^E{}_{ijkl}\, T_{kl} + d_{kij}\, E_k \tag{2.3}$$

$$D_i = d_{ikl}\, T_{kl} + \epsilon^T{}_{ik}\, E_k \tag{2.4}$$

where T_{kl} and S_{ij} are the components of the stress and strain tensors, respectively. Furthermore, $s^E{}_{ijkl}$ is the tensor of compliance under constant electric field, d_{ikl} the piezoelectric constants (in C/N), E_k the electric field and ϵ^T_{ik} the dielectric constant under constant stress. These formulae use classical tensor notations, where all indices $i, j, k, l = 1, 2, 3$ and there is a summation on all repeated indices. The superscripts $_E$ and $_T$ indicate properties measured respectively at constant electric field and at constant stress. Typically the index 3 indicates the polarization direction. Equation 2.3 describes the actuating properties, i.e. the reverse piezoelectric effect, while Equation 2.4 describes the sensing properties, i.e. the direct piezoelectric effect.

There are three main types of piezoelectric transducers, depicted in Figure 2.4: extension actuators, stack actuators and shear actuators.

The extension actuators are the most used kind of actuator in the field of AVC for flexible systems. The actuators are typically bonded to the structure that needs to be damped and rely on the d_{31} coupling coefficients, which makes them elongate (or shrink) in the direction 1, which is the longitudinal direction, in the presence of an external voltage applied along the poling direction 3. These actuators are usually used in pairs. In particular when one of the extension actuators elongates, the other shrinks, so that the structure they are bonded to is subjected to a pure torque. Extension actuators used in pairs are called bimorph actuators, when they are alone they are defined as unimorph actuators.

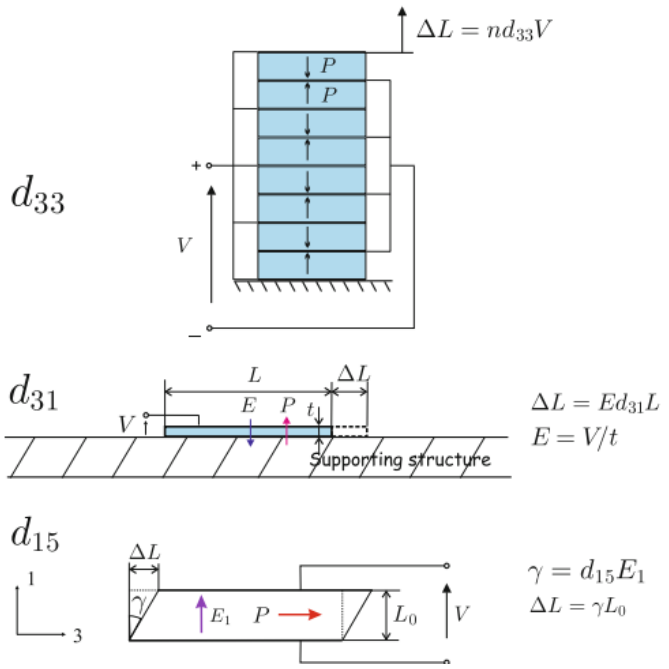

Figure 2.4: Piezoelectric actuators: going from top downwards, piezo stack, extension and shear actuators are illustrated [5]

The stack actuators are piezoelectric actuators that rely on the d_{33} coefficient, which makes them elongate or shrink in the poling direction 3 in presence of an external electric field in the same direction. As the name suggests, they consists of several piezoelectric elements stacked on top of each other. This is done because one single piezoelectric element would not be able to achieve high displacements, but if many of them are grouped together then it is possible to have satisfactory strokes.

The shear actuators rely on the d_{15} or on the d_{24} coupling coefficients, which are generally the largest ones. When an electric field is applied in a direction that is normal with respect to the polarization direction, shear deformation occurs. Therefore, for example, shear actuators based on the d_{15} coefficient give rise to a S_{13} deformation when a voltage is applied in the 1 direction, as can be observed from Figure 2.4. Control strategies involving shear actuators are typically more subjected to model parameter errors [18].

Sensing

Piezoelectric sensors are based on the direct piezoelectric effect, whose constitutive equation is reported in Equation 2.4. As they are deformed, they generate a voltage that can be directly related to the amount of deformation. This voltage is then used in a feedback system to give the information to the controller on how to drive the piezoelectric actuator. Generally, the voltages produced by piezoelectric sensors are very small, therefore amplifiers are usually needed [20]. Furthermore, piezoelectric sensors are typically placed in pairs with the piezoelectric actuators in correspondence of the same degree of freedom, giving rise to collocated control. It is possible to place actuator and sensor at different degrees of freedom, but it is not recommended because it is more complex and it can easily lead to instability, which is already a risk for collocated systems [5]. Finally it is possible to use one single piezoelectric material as both a sensor and an actuator at the same time, giving rise to the so-called self-sensing actuation (SSA). SSA can be classified into two approaches: SSA based on the piezoelectric direct effect and SSA based on the PEA's change of electrical properties. The first approach is more common and aims to separate the charges due to the deformation from those due to the dielectric effect and reconstruct the actuator displacement without the need of an external position sensor [21]. Even though SSA could offer several advantages, such as the "perfect" collocated control, since sensor and actuator would be represented by the same piezoelectric element, it makes systems much more complex and there is high risk of degrading the closed loop performance.

Control
There are many types of controller that can be employed in AVC. Some of the most common ones are represented by feedback solutions like positive position feedback (PPF), direct velocity feedback (DVF) and integral resonant control (IRC). IRC is the simplest kind of controller and it is robust, PPF is typically an effective option and it gives the possibility to control different modes, while DVF is generally not a preferred option since it requires high control effort at all frequencies. For a more detailed description of the possible control alogorithm for AVC the reader is referred to the book [5].

2.1.3. Hybrid damping
The advantages of passive and active damping can be combined by adopting both passive and active control strategies at the same time, giving rise to hybrid damping.

In particular, it is possible to use piezoelectric shunts along to active control of the piezos, as depicted in Figure 2.5, giving rise to so-called Active-Passive-Piezoelectric-Networks (APPN). In this case, the design of the shunt circuit can change with respect to the purely passive case: if the shunt impedance is designed as if the system was completely passive, the control technique would be at the maximum level of robustness; if the shunt design consisted in minimizing a cost function that takes into account not just the robustness of the system but also the performance of the whole control method, then the impedance value could be modified [22] [23].

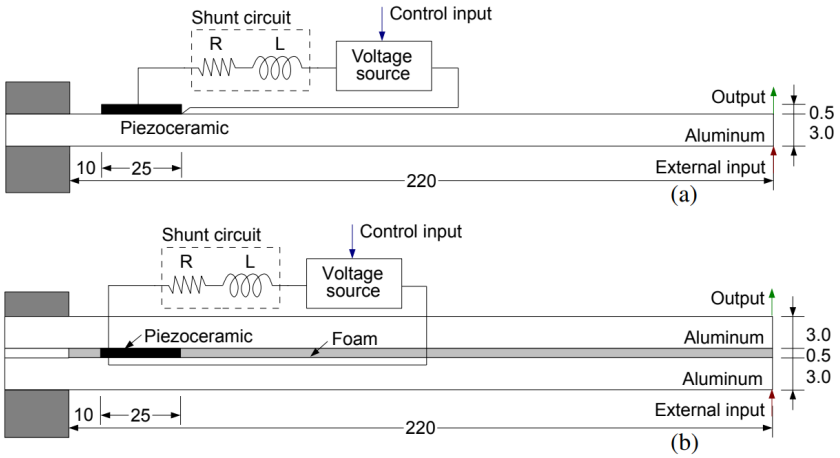

Figure 2.5: Active-Passive-Piezoelectric-Network [18]

2.2. Eddy current damping
Electromagnetic damping devices are becoming increasingly important in the high-tech industry, since they offer many advantages such as the absence of mechanical contact and all the issues it carries like friction wear, typical of conventional dampers. Furthermore, magnetic materials are relatively reliable, thermally stable and can be applied in vacuum [24].

Among all the damping devices that rely on electromagnetism, Eddy current dampers (ECDs) are the most known and used in the field of vibration attenuation in lightweight structures because of their versatility. The basic principle of these dampers consists in electromagnetic induction [17]. When an electrically conductive material plate moves in a space characterized by a magnetic field, an electric field, i.e. a $motional$ electromotive force, is induced on it and, as a consequence, electric currents can be generated. The same phenomenon occurs also when the conductor does not move but it is in a time-varying magnetic field and a $transformer$ electromotive force is generated. Then, these Eddy currents die out thanks to the resistance of the conductive material. Therefore, from the movement of a conductive plate within a magnetic field, created typically by permanent magnets, electric currents and then electric heat can be generated. Applying this principle to a vibrating structure, having conductive material oscillating in a magnetic field, a damping action is generated since the vibrational energy is converted into heat.

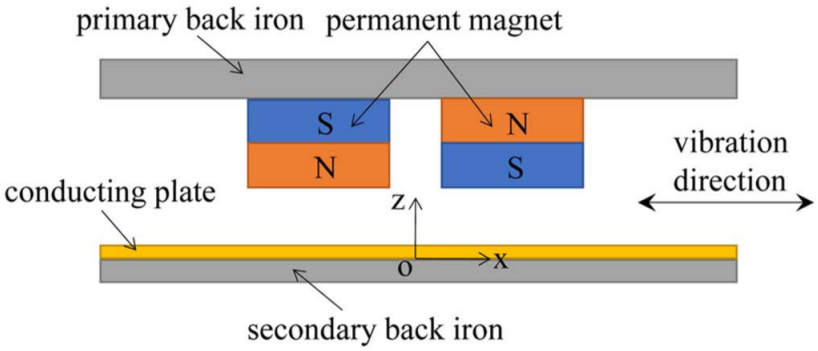

Figure 2.6: Axial ECD [25]

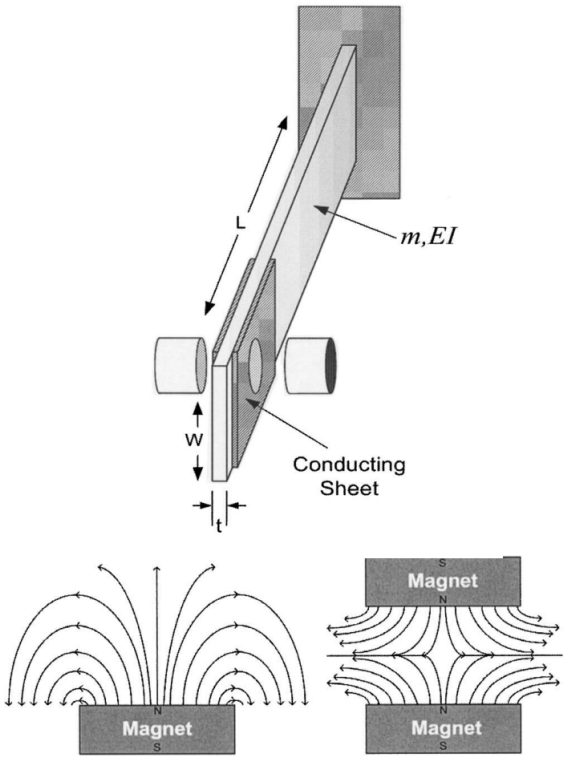

Figure 2.7: Radial ECD: it can be noticed that two repelling magnets give rise to a stronger radial component of the magnetic field than a single one [26]

There are basically two types of Eddy current dampers: ECDs that rely on the ”axial” component of the magnetic field [25] [27], i.e. the component that is in the normal direction with respect to the conductive sheet surface, and ECDs that rely on the ”radial” component [26] [17], i.e. the component of the magnetic field that is in the same plane of the conductive sheet surface. These two different typologies are depicted respectively in Figure 2.6 and in Figure 4.1. According to Lorentz law, the induced Eddy current density **J** is given by conductivity σ of the plate multiplied by the cross product between the velocity **v** of the conductor and the magnetic field **B**:

$$\mathbf{J} = \sigma(\mathbf{v} \times \mathbf{B}) \tag{2.5}$$

Therefore, in axial ECDs the axial component of the magnetic field is the important one to provide damping, since the movement of the conductive plate is perpendicular to it. A similar reasoning holds for radial ECDs.

Several considerations can be done for ECDs. The frequency of movement of the conductive material, i.e. the frequency of vibrations, is in principle directly proportional to the damping force, but at high frequencies the induced currents ”shield” the conductive material from the external magnetic field, worsening the damping action, following a phenomenon called skin depth effect [27]. Therefore, ECDs are typically not effective at high frequencies. Furthermore, the magnetization of the magnets is quadratically proportional to the damping coefficient [24]. Therefore air gaps between elements must be minimized since air has an extremely low magnetic permeability and, as a consequence, it makes the path of magnetic field lines to have a higher reluctance (i.e. a higher ”magnetic resistance”), which in turn makes the magnetic field intensity weaker. Furthermore, since the magnetic field intensity is quadratically proportional to the damping coefficient, it is worth noticing that in radial ECDs, like in the one depicted in Figure 4.1, the radial flux can be enhanced by placing two repelling magnets, instead of just one. Furthermore, another way to increase the damping performance is to include mechanical movement multiplication of the moving part of the ECDs, since larger movements can lead to higher velocities and, as a consequence, to a stronger damping force. Unfortunately, the movement multiplication stages also carry many drawbacks: indeed, pure mechanical ones need maintenance, lubrication, and of course contact, limiting those advantages provided by the eddy current dampers, while new magnetic multiplication stages can be used only at low frequencies otherwise they become totally ineffective [28]. As a last comment, when designing ECDs it is important to consider that the damping action is also proportional to the thickness of the conductive plate, since the electric resistance is inversely proportional to its thickness [17], but it is also true that a thicker plate generally leads to have a larger gap between magnets, which in principle should be minimized. Therefore, a trade-off between plate thickness, magnet dimensions and gaps between magnets needs to made and an optimal configuration can be determined for each specific situation.

Finally, it is worth mentioning that there is the possibility to perform active vibration control using electromagnets [29]. In particular, it is demonstrated that active control of inductors employed in Eddy current dampers gives better performances than passive Eddy current dampers not only at low frequencies but also at high frequencies, since the performance of passive ECDs is degraded because of the skin-depth effect at higher frequencies. However, active ECDs suffer the frequency doubling problem and, as a consequence, the controller architecture needs to be more complex.

3

Piezoelectric-based mechanical design for out-of-plane mode attenuation in flexure mechanisms

In this chapter, the main contribution of this thesis, i.e. the piezoelectric-based design for out-of-plane mode attenuation, is outlined. The proposed solution is validated both analytically and in $COMSOL$. Furthermore, this part of the report is written in a paper format to be self-contained. Therefore, some repetition of the information provided in the previous chapters is present.

Piezoelectric-based mechanical design for out-of-plane mode attenuation in flexure mechanisms

Giovanni Marega

***Abstract*— The most problematic eigenmode in machines involving flexure mechanisms is represented by flexural modes. However, it can be noticed that also out-of-plane modes, that occur in the space outside the nominal plane of movement of the mechanism, can be very important, especially in machines with several and coupled degrees of freedom, like 3D positioning stages. In this paper a new design based on piezoelectric shunt damping is proposed in order to tackle out-of-plane modes of flexure mechanisms, without affecting the capability of attenuating the more common flexural modes. This new concept is validated both analytically and using the FEM software $COMSOL$ and it is shown that attenuations of the order of 15 dB can be achieved. Furthermore, the possibility to add active control to the shunted piezoelectric materials, giving rise to a hybrid control strategy, is explored and it is shown that it results in further increase of the added damping.**

I. Introduction

In the high-tech industry the need to keep pushing the limits of productivity and accuracy of machines is constant. Indeed, a higher productivity generally leads to have the possibility to sell more products and have better turnovers for companies and a higher accuracy increases the quality and reliability of products and industrial processes. However, operating at higher frequencies to push the production, keeping high standards of quality, is challenging, especially considering the fact that compliant flexible mechanisms are increasingly applied in high-tech machines. Indeed, compliant mechanisms offer many advantages such as very low friction, no backlash and no need of lubrication (low maintenance in general). Furthermore, they can be applied in extreme environments, like ultra clean vacuum, they are not susceptible to contaminating particles and, last but not least, they are in principle completely monolithic devices [1].

Therefore, since compliant mechanisms present so many positive aspects, there is the will of using them over classical rigid ones even though they are more susceptible to vibrations. Indeed, vibrations represent a problem that can be solved, at least partially, by using vibration control techniques, known also as damping techniques. These vibration control strategies mainly focus on modes of vibration that occur in the nominal and most compliant direction of motion of flexure mechanisms, known also as flexural modes. In fact, the low stiffness of flexures in their most compliant direction, makes them vibrate very easily, especially when excited in the vicinity of one of their eigenfrequencies. An example of flexural mode is given in Figure 1a.

Another kind of mode of vibration that flexures can undergo is represented by the so-called out-of-plane modes, defined in this way because they consist in unwanted deflections that occur in the normal direction with respect to the expected plane of movement, which is typically very stiff. An example of out-of-plane mode is given in Figure 1b.

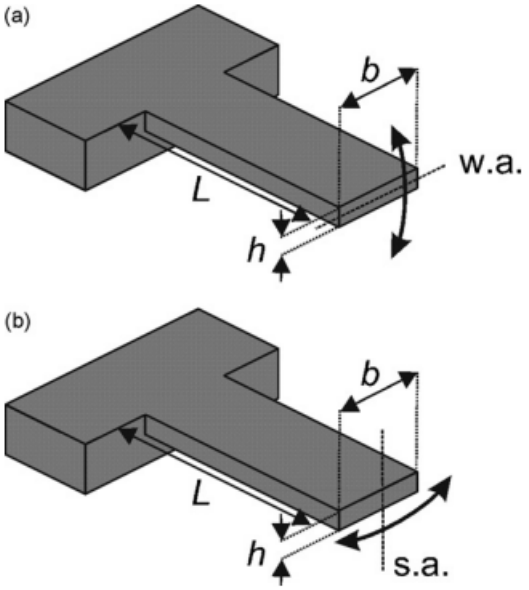

Fig. 1: (a) Flexural bending (b) Out-of-plane bending mode of vibration (w.a. and s.a. denote the “weak” and “strong” axis of the cantilever) [2].

The problems that stiff modes carry are in general underestimated, since flexures are frequently assumed to be perfectly rigid in the out-of-plane direction. Indeed, the literature is quite scarce regarding solutions to avoid such vibrations. Nevertheless, in mechanisms like 3D positioning stages, like the one depicted in Figure 2, out-of-plane deformations could occur: indeed, for example, it can be observed that the presence of the z-axis piezo can make the x and y-axis stages deflect in their out-of-plane direction, especially if the z-axis stage is actuated at the out-of-plane eigenfrequency for either the x or y-axis stages. In such mechanism, the strategy to avoid out-of-plane deflections simply consists in optimizing the stage geometry and the flexure configuration so that the out-of-plane stiffness-to-mass ratios are higher than the actuation stiffness-to-mass ratio [3]. However, this method avoids the problem of out-of-plane modes, rather than solving it. Indeed, the

topology optimization makes the actuation modes, i.e. the flexural modes, occur before than the out-of-plane modes, in an attempt to avoid their excitation. Therefore, if any unexpected force, disturbance or design error occurs, there is not a mechanism able to tackle out-of-plane modes. Another possible method to tackle out-of-plane deflections could be based on the addition of flexure elements able to increase the out-of-plane stiffness, like in the mechanism of (Figure 3), which is an XY positioning stage. This solution is attractive because it also increases the out-of-plane load capacity, i.e. the machine can carry heavy loads without affecting its accuracy. However, the design complexity increases, it is not suitable for more complex mechanisms like 3D positioning stages and it consistently adds unwanted mass and and stiffness in the nominal direction of motion. Finally, the literature on out-of-plane vibration attenuation reports a method based on foams [4], i.e. viscoelastic materials, represented in (Figure 4). This technique is interesting, since viscoelastic damping is suitable for high frequencies, where out-of-plane modes are typically to be found. However, it strongly depends on temperature and frequency and it cannot be employed in vacuum do to out-gassing. Moreover, similarly to the previous concept of (Figure 3), it adds undesired mass and stiffness.

Therefore, out-of-plane modes in flexures represent a problem that stills need to be discussed in depth and new solutions may be helpful. Indeed, if flexures are part of a complex mechanism that is excited in many directions, like 3D positioning stages, they may deform consistently also in the stiff direction if excited in correspondence of out-of-plane eigenfrequencies. Furthermore, the problem of out-of-plane modes is expected to become more and more important in the future: indeed, high-tech machines are pushed to become even more complex, fast and lightweight, increasing the risk of dealing with unwanted and unexpected vibrations besides the more common flexural modes.

Thus, in this work a new design which gives the possibility to dampen out-of-plane modes besides flexural ones is proposed. In particular, the vibration control strategy is based on piezoelectric materials. Therefore, section II is devoted to give a background knowledge on damping techniques involving such materials. In particular, the accent is posed on the vibration control strategy known as "piezoelectric shunt damping". This is done because this damping method is passive, i.e. it does not require any external power supply or controllers, and at high frequencies, where out-of-plane modes are supposed to be found, passive damping is preferred over active damping, since the latter could be influenced by spillover effects and bandwidth limitations. Then, in section III a design concept based on piezoelectric materials for the problem of out-of-plane deflections is illustrated and in section IV it is modeled analytically. Subsequently, in section V a new simplified design is introduced in order to showcase the proposed principle of damping and in section VI it is modeled both analytically and in $COMSOL$. Finally, the paper is concluded and recommendations for future work are put forward.

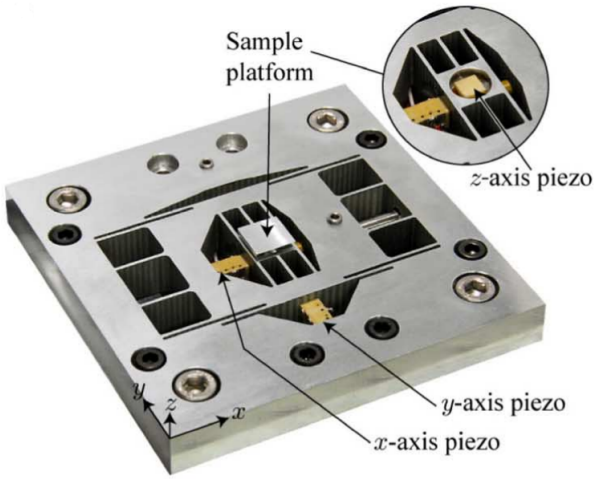

Fig. 2: 3D positioning stage [3]

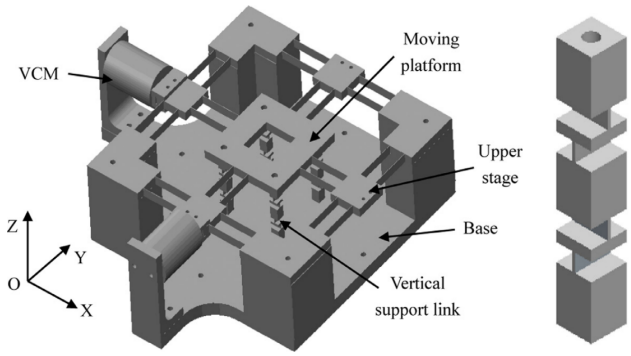

Fig. 3: 2D-positioning stage with increased out-of-plane stiffness. On the right side there is a zoom of the flexure mechanism used to increase the out-of-plane stiffness. [5]

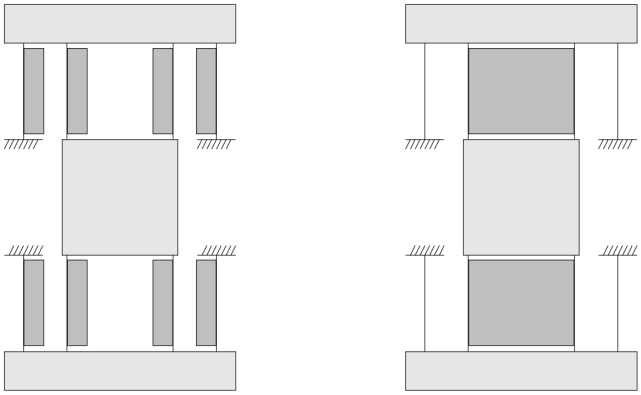

Fig. 4: Four-flexure mechanism with foams for out-of-plane vibration attenuation [4]

II. Background knowledge

In this section, the necessary preliminary information is introduced. First, the piezoelectric effect is described. Then,

the various modes of operations of piezoelectric materials are outlined. Finally, passive, active and hybrid damping based on piezoelectricity is presented.

A. Introduction on piezoelectricity

In the recent years, a new class of materials, defined as "smart materials", is contributing to give rise to new damping methods. These special materials have the capability to couple different physical domains, giving the opportunity to transform energy in different forms [6].

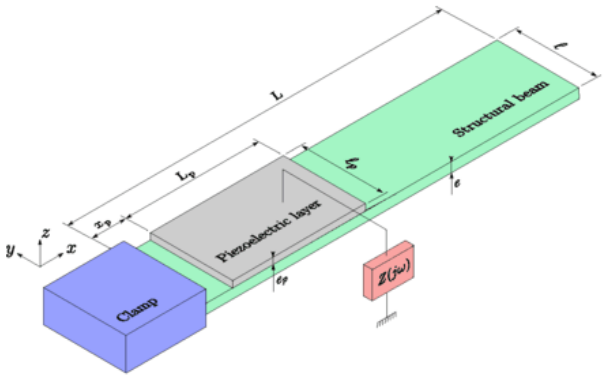

Fig. 5: Schematic of a smart piezoelectric-shunted beam [7]

Among the smart materials, piezoelectric materials are the most used. In fact, these materials can be used for both sensing, relying on the direct piezoelectric effect, and actuation, using the inverse piezoelectric effect [8].

Piezoelectric materials couple the physics of mechanics and electrstatics. In particular, piezoelectricity is the phenomenon that characterizes materials that originate electric charges once they are deformed (direct pizoelectric effect) and that, viceversa, give rise to changes to their dimensions as they are subjected to external electric fields (inverse piezoelectric effect). The mathematical formulation of the piezoelectric effect is given by the following equations:

$$S_{ij} = {s^E}_{ijkl}\, T_{kl} + d_{kij}\, E_k \tag{1}$$

$$D_i = d_{ikl}\, T_{kl} + {\epsilon^T}_{ik}\, E_k \tag{2}$$

where T_{kl} and S_{ij} are the components of the stress and strain tensors, respectively. Furthermore, ${s^E}_{ijkl}$ is the tensor of compliance under constant electric field, d_{ikl} the piezoelectric constants (in C/N), E_k the electric field and ϵ^T_{ik} the dielectric constant under constant stress. These formulae use classical tensor notations, where all indices $i, j, k, l = 1, 2, 3$ and there is a summation on all repeated indices. The superscripts ^{E} and ^{T} indicate properties measured respectively at constant electric field and at constant stress. Typically the index 3 indicates the polarization direction. Eq. (1) describes the actuating properties, i.e. the inverse piezoelectric effect, while Eq. (2) describes the sensing properties, i.e. the direct piezoelectric effect. An illustration on the 1-2-3 direction convention is provided in Figure 8.

Piezoelectric materials can be used as strain sensors when they are mechanically bonded to a deforming structure and rely on the direct piezoelectric effect. Indeed, the deformation occurs also for the piezoelectric material, giving rise to electric charges on its surfaces, whose amount can be linearly related to the amount of deformation. On the contrary, the piezoelectric actuators are based on the inverse piezoelectric effect [6].

B. Vibration control with piezoelectric materials

As just mentioned, piezoelectric materials generate electric charges if they are bonded to a vibrating structure. This phenomenon, consisting on the direct piezoelectric effect, can be exploited in two ways in the field of vibration control. On the one hand, it can be used to perform active vibration control. In particular, it gives the possibility to create a deformation sensor, as just stated in the introduction: then, the data coming from the sensor can be used in a feedback loop to control another piezoelectric material, used as an actuator relying on the inverse piezoelectric effect, in order to perform a counter-action against the vibrations. On the other hand, it is possible to rely on the direct piezoelectric effect in order to create a passive damping technique, called piezoelectric shunt damping: if an electric circuit is build around the piezoelectric element, the charges that it creates because of the deformation give rise to an electric current, which in turn dies out thanks to the impedance of the circuit. Therefore, starting from vibrational energy, electric energy is produced, which is in turn dissipated in the electric circuit, giving rise to a damping effect.

Overall, piezoelectric materials can be used in both a passive and an active way in order to attenuate vibrations. Furthermore, it is possible to combine passive and active use of such materials, giving rise to an hybrid structure. In the following paragraphs, such control strategies are described in more detail, giving a particular emphasis on the passive damping method.

C. Piezoelectric shunt damping

The most common passive control method involving piezoelectric materials is represented by the so-called piezoelectric shunt damping, which is schematically illustrated in Figure 5. This technique consists in connecting electric or electronic circuits (indicated by impedance $Z(\omega)$ in Figure 5) to the electrodes of a piezoelectric transducer bonded to a vibrating structure [7], defined also as "smart" structure because of the presence of the "smart" piezoelectric material. In this way, the mechanical vibrations cause the piezoelectric material to generate electric charges according to the direct piezoelectric effect and these charges generate in turn an electric current in the circuit, composed by the piezoelectric transducer (which can be seen as a capacitor) and by the impedance $Z(\omega)$. Therefore, the mechanical vibrational energy is converted, partially, into

electric energy which is then dissipated in the circuit with a proper selection of the impedance $Z(\omega)$.

The characteristics of the electric circuit, the material properties and the dimensions and positions of the piezoelectric elements determine the effectiveness of the damping action. As a general guideline, in the case of flexible structures such as cantilever beams, the piezoelectric patches should be placed at the locations of maximum modal strain energy [9]. For example, in Figure 5 it can be seen that the piezo is placed next to the clamp, which is where the maximum strain can be observed as the beam bends downwards at the first eigenfrequency.

In the literature many kinds of electric shunt circuits are proposed and studied, some of them are simple and give the possibility to dampen only one mode, while others are more complex and can dampen several modes: for a detailed illustration of the possible shunt circuits, the reader is referred to the review of [10]. One of the most studied ones is the series RL-shunt circuit: if the electrical eigenfrequency is properly tuned, it leads to an effective means of achieving vibration attenuation. Indeed, given the inherent capacitance of the piezoelectric transducer, C_p, the two other parameters of the resonant circuit can be tuned with respect to a particular natural frequency of the mechanical structure for achieving minimum vibration amplitudes in the vicinity of that frequency. The formulae for determining the optimal values L_{opt} and R_{opt} for the RL-shunt circuit are [11]:

$$R_{opt} = \sqrt{2}\frac{K_i}{(1+{K_i}^2)C_p\omega_n} \tag{3}$$

$$L_{opt} = \frac{1}{(1+{K_i}^2)C_p{\omega_n}^2} \tag{4}$$

where ω_n is a normalization frequency, chosen typically very close to the structural eigenfrequency, C_p is the electric capacitance of the piezoelectric transducer and K_i is the electromechanical coupling coefficient, which can be identified from experimentally measured open-circuit and short-circuit natural frequencies but also estimated analytically, as done for example in [12].

It is worth noticing that the value for the inductance has to be generally high. Therefore, instead of using real and bulky inductors, synthetic inductors that rely on operational amplifiers are often preferred [13]. Then, the piezoelectric shunt is said to be semi-passive, since such electronic devices are active but they are used to create a circuit that behaves like a passive one.

Referring to the system of Figure 5, it can be demonstrated that the vibration amplitude of the tip of the cantilever beam varies with the frequency of excitation following the curves plotted in figure Figure 6. Therefore, it can be observed that the system becomes very similar to the one with a tuned mass damper if the shunt impedance has an inductance, since two resonance peaks are present. In addition, it can also be noticed that a proper selection of the components in the shunt is essential to achieve high vibration attenuation.

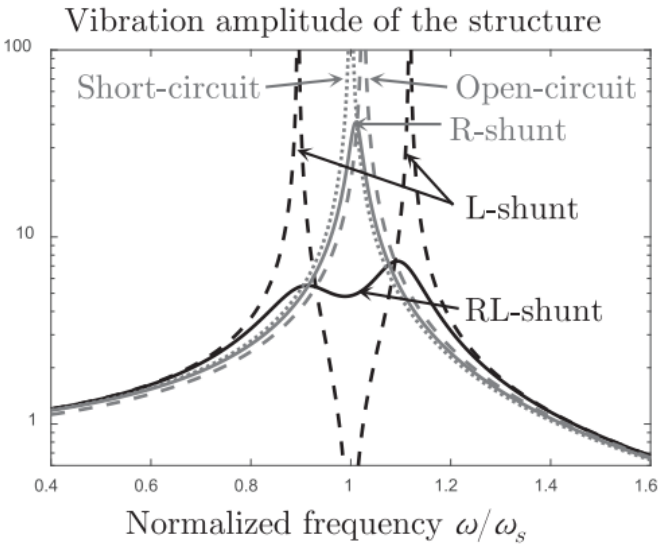

Fig. 6: Typical frequency response function of a shunted piezoelectric material bonded to a vibrating structure [10]

Furthermore, it can be observed that the inherent capacitance C_p of the piezo represents an obstacle for the dissipation of the electric energy, since it represents a negative impedance, equal to $\frac{-j}{\omega C}$. Indeed, the RL shunt can effectively damp eigenmodes since the negative impedance that characterizes the capacitance C_p is compensated by the positive impedance of the inductance L, equal to $j\omega L$ in correspondence of the electrical eigenfrequency. However, this compensation occurs only at the eigenfrequency, therefore synthetic negative capacitance circuits, made using OpAmps, are often used to eliminate the capacitive behavior of the shunt [14]. This solution, however, carries the risk of instability.

Moreover, as already mentioned, the effectiveness of piezoelectric shunt damping strongly decreases if the electric impedance is not tuned properly. Therefore, adaptive shunt circuits, which are able to perform online adaptation of their impedance, can be created in order to solve the detuning problem [15]. Even though this solution can give satisfactory results, its implementation is complex and requires plenty of electronic components.

Overall, piezoelectric shunt damping represent a new and very interesting field of research, since it represents a lightweight and effective solution to attenuate vibrations in flexible systems and its limitations, such as the detuning problem of the shunt impedance, can be circumvented.

D. Piezoelectric active vibration control

As already mentioned, piezoelectric materials deform if subjected to external electric fields. Therefore, if they are bonded to a vibrating structure, it is possible to dampen vibrations by applying a proper and controlled voltage across the piezoelectrics, based on the sensed deformation of the structure, such that the smart material is pushed to deform in a way that opposes the unwanted vibrations. A typical active vibration control (AVC) method based on piezoelectricity is represented in Figure 7, that depicts a vibrating cantilever beam. Similarly to the passive piezoelectric shunt damping method, also in AVC the piezoelectric actuators are supposed to be placed in correspondence of the locations with the maximums of modal strain energy, i.e. at the antinodes of eigenmodes. In this way, the controllability and the observability of the system are maximized. Furthermore, it is worth noticing that the piezoelectric sensor and actuator pair is typically collocated, i.e. the piezos are located in the same longitudinal coordinate of the cantilever beam, as shown in Figure 7. This gives rise to a collocated system, making it more stable and robust. Non-collocated systems are in general avoided as they require more energy, can induce instability and they are harder to implement than collocated ones [6].

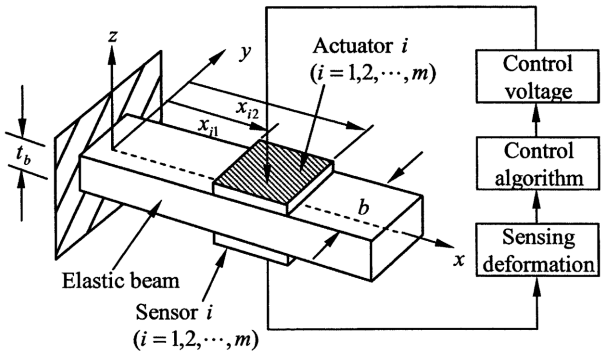

Fig. 7: Typical AVC layout based on piezoelectric components [16]

The deformation induced on the piezo could be of basically three types, giving rise to either elongating actuators (relying on the d_{31} coefficient), stack actuators (based on d_{33} coefficient) and shear actuators (based on either the d_{15} or the d_{24} coefficient), as depicted in Figure 8. For example, in the vibration control structure depicted in Figure 7, elongating actuators relying on the d_{31} are used to tackle flexural modes.

There are many types of controller that can be employed in AVC. Some of the most common ones are represented by feedback solutions like integral resonant control (IRC), direct velocity feedback (DVF) and positive position feedback (PPF). IRC is the simplest kind of controller and it is robust. DVF is generally not a preferred option since it requires high control effort at all frequencies. PPF is typically an effective, stable and easy to implement option and it gives the possibility to control different modes [6].

In particular, the typical transfer function of a PPF controller is given in Eq. (5).

$$PPF = \frac{-g}{s^2 + 2\zeta_f \omega_f s + (w_f)^2} \tag{5}$$

The controller has three variables: g (gain), ω_f (cut-off frequency) and ζ_f (damping ratio). For the most effective action, the cut-off frequency should be tuned close to the resonance frequency of the vibration mode that needs to be damped. The two remaining variables, gain and damping ratio, can be used to tune the controller to reach the desired effect.

For a more detailed description of the possible control alogorithm for AVC the reader is referred to the book [6].

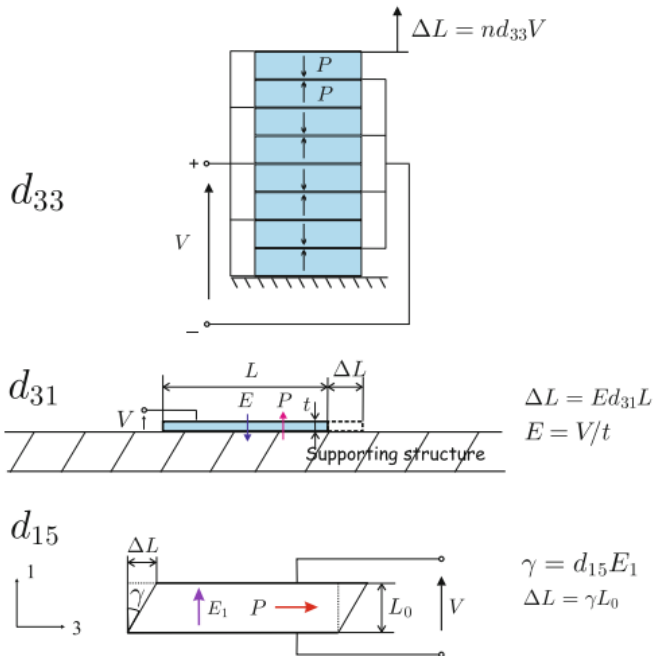

Fig. 8: Piezoelectric actuators. Going from top downwards, piezo stack, extension and shear actuators are illustrated. The P vector indicates the polarization, which is conventionally along direction 3, while E stands for the electric field. [6]

E. Piezoelectric hybrid vibration control

The advantages of passive and active damping can be combined by adopting both passive and active control strategies at the same time, giving rise to hybrid damping. In particular, it is possible to use piezoelectric shunts along to active control of the piezos, as depicted in Figure 9, giving rise to so-called Active-Passive-Piezoelectric-Networks (APPN). In this case, the design of the shunt circuit can change with respect to the purely passive case: if the shunt impedance is designed as if the system was completely passive, the control technique would be at the maximum level of robustness; if

the shunt design consists in minimizing a cost function that takes into account not just the robustness of the system but also the performance of the whole control method, then the impedance value can be modified [17] [18].

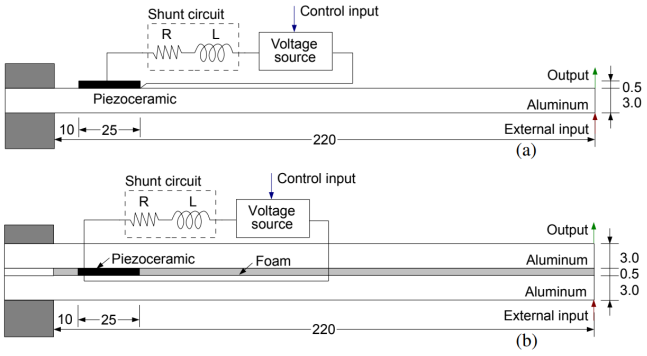

Fig. 9: Active-Passive-Piezoelectric-Network [19] with (a) extension patches and (b) shear patches

III. Model concept

As previously said, one of the suitable options to tackle out of plane modes is represented by the use of piezoelectric materials. In order to illustrate the piezoelectric-based concept on how mitigate out-of-plane modes in flexures, the flexure mechanism of Figure 10 is considered. Such system represents a 4-flexure mechanism, found in many high-tech machines such as 3D positioning stages, like the one of Figure 2. The geometrical parameters of Figure 10 are given in Table I. An eigenfrequency analysis of the mechanism is performed and the results are depicted in Figure 11. It can be noticed that the first mode is a flexural mode and, as already specified in the introduction, this kind of deflection typically represents the major problem for vibrations in flexures, since it takes place in the compliant transverse plane of the flexure and it is easy to excite. However, also other modes are present. In particular, the next three modes are of out-of-plane nature, since they do not belong to the nominal plane of movement of the flexures. Therefore, also out-of-plane modes can represent an important issue, especially at high frequencies and for machines having coupled degrees of freedom like 3D positioning stages. Moreover, considering that the first flexural mode is a kind of "desired" mode (since it gives the possibility to move the end-effector (EE) without a lot of effort, not compromising the accuracy of the motion), the first "problematic" eigenmode of the mechanism of Figure 10 is represented by an out-of-plane mode.

Parameter	Value	Unit	Description
h	0.015	m	Height of the flexure substrate
b_s	0.001	m	Width of the flexure substrate
l	0.05	m	Lenght of the flexure substrate
W_{ee}	0.08	m	Width of the EE
L_{ee}	0.08	m	Lenght of the EE

TABLE I: Geometrical parameters of the system of Figure 10

At this point, having highlighted the kind of system to consider in order to find a control strategy for out-of-plane

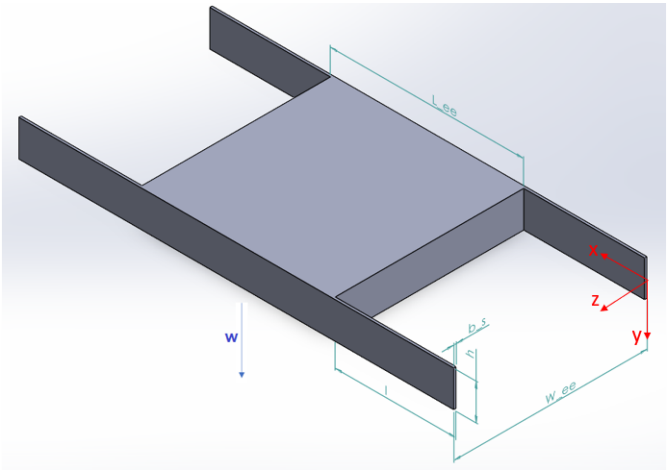

Fig. 10: Typical 4-flexure mechanism whose out-of-plane vibrations need to be suppressed

mode attenuation, it is time to illustrate the concept of the piezoelectric-based solution. In order to attenuate the first out-of-plane mode of the 4-flexure mechanism, depicted in Figure 11b, piezoelectric materials, i.e. patches, could be placed on each flexure in the way described in Figure 13, giving rise to the mechanism of Figure 14. On each side of the flexures, four different patches are placed and shunted with four different and independent electrical circuits. The patches are supposed to be polarized and shunted in the direction of the thickness, so that when the out-of-plane deformation occurs they give rise to a voltage dependent on the d_{31} coefficient: then, this voltage gives rise to a current that dies out in the shunt impedance, leading to a damping effect.

The necessity of using four patches is motivated by the fact that the structure is going to deform in the way depicted in Figure 12 at the first out-of-plane eigenfrequency and 4 patches are necessary in order to avoid charge cancellation [20] [6] and cover the whole surface of the flexure at the same time, maximizing the coupling between the electrical and the mechanical domains. Indeed, piezoelectric materials generate both positive and negative voltages dependent on the strain direction and if both positive and negative deformations are present in the area covered by one of the patches there is partial or even total charge compensation. Therefore, the patches should be placed in such a way that they do not include both areas where there is extension and areas where there is compression.

Furthermore, it is worth noticing that the configuration proposed in Figure 13, from the point of view of a single flexure, does not lead to optimal weight to damping ratio, since the patches are present also in the central part of the flexure, around $x = l/2$, where the strains are small: however, it is also true that, from a global point of view, the weight added by the patches is negligible compared to the weight of the whole structure with the end-effector (which has dimensions equal to L_{ee} x H_{ee} x h, where the subscript $_{ee}$ stands for end-effector).

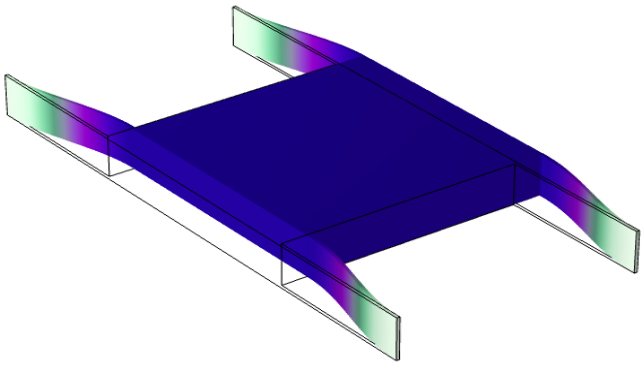

(a) 1st mode: flexural

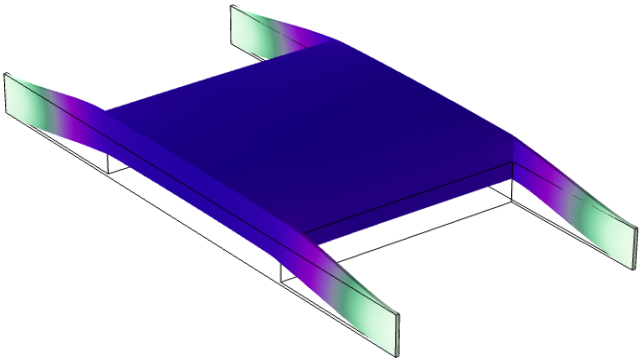

(b) 2nd mode: out-of-plane

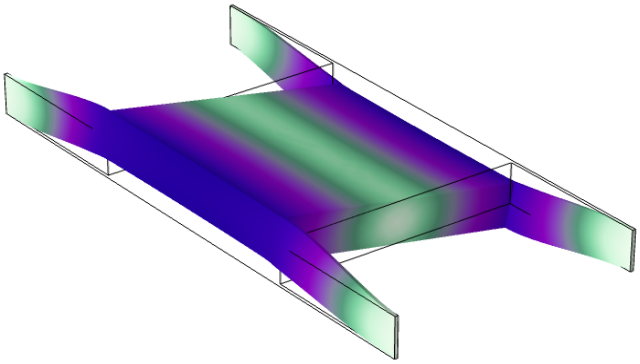

(c) 3rd mode: out-of-plane

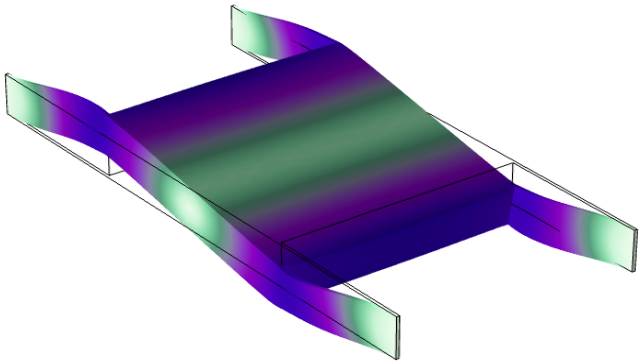

(d) 4th mode: out-of-plane

Fig. 11: First four eigenmodes for the mechanism of Figure 10

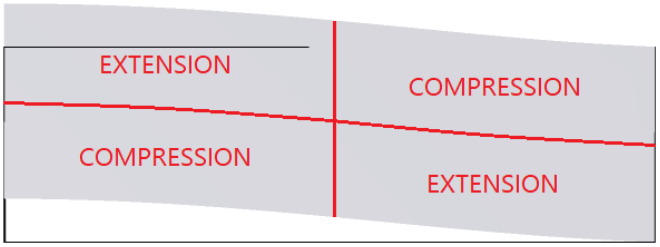

Fig. 12: First out-of-plane mode with focus on the deformation on the flexures

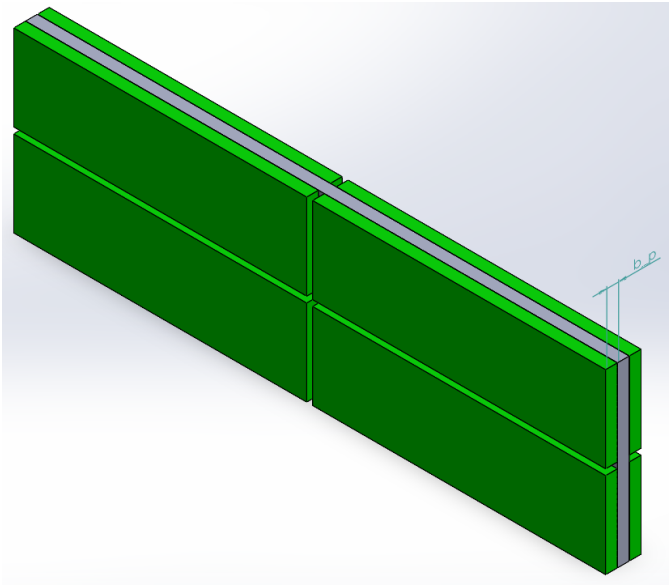

Fig. 13: Proposed disposition of piezoelectric patches, highlighted in green, to dampen out-of-plane vibrations

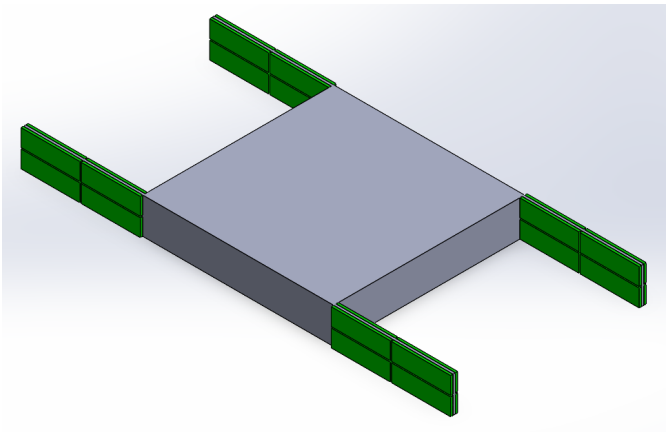

Fig. 14: Global design for out-of-plane mode attenuation using piezoelectric materials

Moreover, this configuration of the patches leads to a uniform section of the smart flexure and the analytical model of the proposed design can be simplified. Finally, it is important to notice that this configuration of piezoelectric patches does not preclude the possibility to tackle also the more common flexural modes. Indeed, their polarization is set to be the one typical of extension actuators (i.e. the polarization is directed along the thickness of the patch), which are widely used for flexural mode attenuation. The only difference is that, in the case of out-of-plane mode damping, the piezoelectric elements need to be divided along the longitudinal direction, but this division does not affect the capability to tackle also flexural modes.

IV. Analytical model

At this point, having defined the system supposed to represent a solution for out-of-plane vibration attenuation, an analytical model needs to be developed in order to come up with a first mathematical description and approximation of its effectiveness.

As described in [12],[21], the behavior of a smart beam can be modeled using Hamilton's principle, starting from the definition of the potential energy, kinetic energy and external work applied to the system. Then, Rayleigh-Ritz procedure and Euler-Bernoulli beam theory are applied. Therefore the behavior of the system of Figure 14, around one if its resonance frequencies can be described by considering the mode shape function $\phi(x)$ of the corresponding eigenmode, since the contribution of the other modes would be relatively negligible. Then, the state-space model of the 4-flexure mechanisms with piezoelectric patches can be reduced to the a scalar form having 3 coupled equations.

The xyz coordinate system that is used in the following derivations is represented in Figure 10.

A. Derivation of the mathematical model

As just mentioned, Hamilton's principle can be applied in order to model piezoelectric materials bonded to a vibrating structure. Then, it is necessary to have formulations for the potential energy U, kinetic energy T and external work applied to the system $f\delta x$:

$$U = \frac{1}{2}\int_{V_s} S^T T dV_s + \frac{1}{2}\int_{V_p} S^T T dV_p - \int_{V_p} E^T D dV_p \quad (6)$$

$$T = \frac{1}{2}\int_{V_s} \rho_s \dot{u}^T \dot{u} dV_s + \frac{1}{2}\int_{V_p} \rho_p \dot{u}^T \dot{u} dV_p \quad (7)$$

$$f\delta x = \sum_{i=1}^{nf} \delta u(x_i)\cdot f_i(x_i) - \sum_{j=1}^{nq} \delta v \cdot q_j \quad (8)$$

The subscripts s and p stand respectively for the substrate, represented by the spring-steel flexure, and the piezoelectric elements. In particular, V_s indicates the volume of all the flexures while V_p the volume of all the piezoelectric components. Furthermore, S is the strain, T is the stress, E is the electric filed, D is the electric displacement, V is the volume, u is the displacement, x is the position along the beam, v is the applied voltage, q is the charge, ρ is the density and f is the applied force.

It can be noticed that it is possible to use the constitutive equations for piezoelectric materials and have a more insightful equation for the potential energy. In particular, the characteristic equation for piezoelectric material, already reported in the previous section, can be expressed in the following manner:

$$\begin{bmatrix} T \\ D \end{bmatrix} = \begin{bmatrix} c^E & -e^T \\ e & \epsilon^S \end{bmatrix} \begin{bmatrix} S \\ E \end{bmatrix} \quad (9)$$

where T and S are again the stress and strain tensors, respectively, while D represents the so-called electric displacement, expressed in C/m^2, and it represents the density of electric charges on the surfaces of the piezoelectric element. Furthermore, c^E is the stiffness tensor under constant electric field, e^T is the piezoelectric coupling coefficient, E the electric field and ϵ^S the dielectric constant under constant strain.

Then, the potential energy equation becomes the following:

$$\begin{aligned} U = \frac{1}{2}\Bigg[& \int_{V_s} S^T c_s S dV_s + \int_{V_p} S^T c^E S dV_p \\ & + \int_{V_p} S^T e^T E dV_p - \int_{V_p} E^T e S dV_p \\ & - \int_{V_p} E^T \epsilon^s E dV_p \Bigg] \end{aligned} \quad (10)$$

At this point, it is possible to apply Hamilton's principle, which states that it is possible to obtain the equations of motion of a system by solving the variational integral $V.I.$ stating that the energy of a system does not change in time. Therefore:

$$V.I. = \int_{t_1}^{t_2} \left[\delta T - \delta U + f\delta x\right] dt = 0 \quad (11)$$

which leads to:

$$\begin{aligned} V.I. = \int_{t_1}^{t_2} \Bigg[& \int_{V_s} \rho_s \delta\dot{u}^T \dot{u} dV_s + \int_{V_p} \rho_p \delta\dot{u}^T \dot{u} dV_p \\ & - \int_{V_s} \delta S^T c_s S dV_s - \int_{V_p} \delta S^T c^E S dV_p \\ & + \int_{V_p} \delta S^T e^T E dV_p + \int_{V_p} \delta E^T e S dV_p \\ & - \int_{V_p} \delta E^T \epsilon^s E dV_p + \sum_{i=1}^{nf} \delta u(x_i)\cdot f_i(x_i) \\ & - \sum_{j=1}^{nq} \delta v \cdot q_j \Bigg] dt = 0 \end{aligned} \quad (12)$$

Subsequently, three assumptions are made in order to simplify the model. First, Rayleigh-Ritz procedure is applied,

which assumes and defines the displacement of a beam-like structure as the summation of modes in the beam and a temporal coordinate. Furthermore, if the excitation frequency is assumed to be very close to one of the eigenfrequencies, it is possible to consider only one of the eigenmodes, since the influence of the others would be negligible. Therefore, using Rayleigh-Ritz procedure, the displacement u of the beam can be expressed in the following way:

$$u(x,t) = \phi(x)w(t) \tag{13}$$

ϕ is the assumed mode shape function of the structure. More precisely, it is the assumed mode shape function of the flexure having the xyz coordinate system located at its base, as represented in Figure 10, and it is applied also to the other flexures since they are all supposed to deform identically at the first out-of-plane mode, as can be observed in Figure 11b). The mode shape function ϕ can be set to satisfy any combination of boundary conditions and $w(t)$ is the temporal coordinate of the displacement.

The second assumption made is to apply the Euler–Bernoulli beam theory, which assumes that the strain is linearly related to the distance from the neutral axis, defined as:

$$S = -y\frac{\partial^2 u(x,t)}{\partial x^2} = -y\phi(x)w(t) \tag{14}$$

As done for the formulation of the displacement u, the stress S defined in Eq. (14) is referred to the flexure having the coordinate system where it is clamped and the stress in all the other flexures is assumed to be of the same kind.

The third and last assumption is that the electric potential across the piezoelectric element is constant. This assumption also indicates that no field is applied to the beam, which designates the beam to be inactive material. Therefore, the electric potential E can be expressed in the following way:

$$E = \psi(z)v(t) \tag{15}$$

where,

$$\psi(x,y) = \begin{cases} 1/b_p & 0 < y < h/2 \quad 0 < x < l/2 \\ -1/b_p & -h/2 < y < 0 \quad 0 < x < l/2 \\ 1/b_p & -h/2 < y < 0 \quad l/2 < x < l \\ -1/b_p & 0 < y < h/2 \quad l/2 < x < l \end{cases} \tag{16}$$

The sign of ψ reflects the fact that the polarization direction on the patches undergoing the same kind of deformation is set to be the same and, at the same time, opposite to the polarization direction of the other patches, that deform in the opposite way.

As already done in Eq. (13) and Eq. (14), the aformentioned expression refers to the flexure having the reference frame and it is applied also to the other flexures.

Using these assumptions we can simplify the variational integral to include terms that represent physical parameters and the system can be described by the following coupled equations:

$$(M_s + M_p)\ddot{w} + C\dot{w} + (K_s + K_p)w - 32\,\theta v = F \tag{17}$$

$$C_p\dot{v} + \theta\dot{w} = i \tag{18}$$

where,

$$M_s = 4\int_{V_{s1}} \rho_s\phi(x)\phi(x)\,dV_{s1} + M_{ee} \tag{19}$$

$$M_p = 4\int_{V_{p1}} \rho_p\phi(x)\phi(x)\,dV_{p_1} \tag{20}$$

$$K_s = 4\int_{V_{s1}} y^2\phi''(x)\phi(x)''c_s\,dV_{s_1} \tag{21}$$

$$K_p = 4\int_{V_{p1}} y^2\phi''(x)\phi(x)''c_p\,dV_{p_1} \tag{22}$$

$$M = M_s + M_p, K = K_s + K_p \tag{23}$$

$$C = 0.02 \times 2\sqrt{KM} \tag{24}$$

$$\theta = \int_{V_{p11}} y\phi''(x)e^T\psi(x,y)\,dV_{p_{11}} \tag{25}$$

$$C_p = \int_{V_{p11}} \psi^T(x,y)\epsilon\psi(x,y)\,dV_{p_{11}} \tag{26}$$

V_{s1} is the volume of the substrate for the flexure located at the origin of the coordinate system, V_{p1} the volume of all the piezoelectric elements in the flexure, V_{p11} the volume of just one of the piezoelectric elements in the flexure. K represents the stiffness matrix while M represents the mass matrix. Furthermore, w is the displacement of the mechanical degree of freedom taken into consideration, i.e. the out-of-plane displacement. q is the electric charge, i the electric current, ρ the density, c the Young's modulus, e the piezoelectric coupling coefficient (equal to $d_{31}c_p$), ϵ the dielectric constant and M_{ee} the mass of the end-effector.

In most cases, the amount of inherent damping in a structure is less than 2% structural [22]. Therefore, in the aforementioned coupled equations the term C, defined in Eq. (24), stands to reflect this kind of damping.

θ and C_p represent respectively the coupling term and the capacitance of each piezoelectric element. In principle, every patch could have a different coupling with the structure (and also a different capacitance) but in this case the patches are placed in a symmetric way and in regions having equal strain magnitudes, as it can be deduced from the mode shape function ϕ reported in Eq. (27).

It is worth noticing that the expressions for the mass and stiffness terms have the integral multiplied by 4. Indeed, the

expression in the integral gives the respective value for just one flexure. In the case of the mass term for the substrate, also the mass of the end-effector is considered. Furthermore, in Eq. (17), the coupling term θ is multiplied by 32, reflecting the fact that there are 32 piezoelectric elements in total.

As already mentioned, the mechanical side of each smart flexure is modeled as a single Euler-Bernoulli beam element. Then, following for example the same procedure as [23], the assumed mode shape function ϕ, considering that each flexure can be considered clamped-clamped for the out-of-plane motion, results to be the following:

$$\phi = 3\left(\frac{x}{l}\right)^2 - 2\left(\frac{x}{l}\right)^3 \tag{27}$$

This mode shape function, even though it results from a displacement field assumed to have a third grade polynomial formulation, which may not be as accurate as assuming sinusoidal forms, reflects with good accuracy the situation which is object of study in this work. Indeed, for instance, using the aforementioned mode shape function, the stiffness of just one flexure, equal to $K_s/4$, is determined to be equal to:

$$K_s/4 = \frac{12EI_s}{l^3} \tag{28}$$

which is the same expression obtained in many other publications, such as [24], for a beam in clamped-clamped boundary conditions and, as already stated, in the configuration considered in this work each flexure can be considered as clamped-clamped for the first out-of-plane mode. In Eq. (28), I_s represents the moment of inertia of the flexure substrate.

Then, once the mode shape function ϕ is identified and the geometrical and physical parameters of the system are known, as reported in Table I and Table II, it is possible to determine the outcome of Eq. (19) - Eq. (26):

$$M_s = 4\rho_s h b_s\left(\frac{9l}{5} + \frac{4l}{7} - 2l\right) + \rho_s h W_{ee} L_{ee} \tag{29}$$

$$M_p = 8\rho_p h b_p\left(\frac{9l}{5} + \frac{4l}{7} - 2l\right) \tag{30}$$

$$K_s = 4c_s b_s \frac{h^3}{l^3} = \frac{12EI_s}{l^3}, I_s = b_s\frac{h^3}{12} \tag{31}$$

$$K_p = 8c_p b_p \frac{h^3}{l^3} = \frac{12EI_p}{l^3}, I_p = 2b_p\frac{h^3}{12} \tag{32}$$

$$\theta = -\frac{3}{16l} d_{31} c_p h^2 \tag{33}$$

$$C_p = \epsilon_r \epsilon_0 \frac{hl}{4b_p} \tag{34}$$

Parameter	Value	Unit	Description
b_p	0.001	m	Piezoelectric patch width
c_s	68	GPa	Young's Modulus of the substrate
c_p	210	GPa	Young's Modulus of the piezos
ρ_s	7800	kg/m^3	Density of the substrate
ρ_p	7500	kg/m^3	Density of the piezos
ϵ_r	3130	/	Relative magnetic permeability
ϵ_0	$4\pi 10^{-7}$	$C^2/(Nm^2)$	Dielectric constant of vacuum
d_{31}	-274 10^{-7}	m/V	Coupling coefficient

TABLE II: Geometrical and physical parameters of the substrate structure, made of spring steel, and of the piezoelectric material, which is assumed to be PZT-5H

B. Addition of the shunt circuit

The modeling of the smart flexure presented previously illustrates a situation where piezoelectric elements are bonded to a compliant mechanism. Therefore, in order to model a situation where also a shunt circuit is present and built around the piezoelectric patches, it is necessary to add a third equation next to Eq. (17) and Eq. (18) which describes the fact that the voltage across the piezoelectric element, considerable as a capacitor, is equal to the voltage across the shunt impedance with a minus sign in front, according to Kirchoff first law. Therefore, the system of Figure 14 equipped with shunt circuits can be described by the following three coupled equations:

$$(M_s + M_p)\ddot{w} + C\dot{w} + (K_s + K_p)w - 32\,\theta v = F \tag{35}$$

$$C_p\dot{v} + \theta\dot{w} = i \tag{36}$$

$$V = -ZI \tag{37}$$

where Z is the shunt impedance and V and I are respectively the voltage and the current expressed in the Laplace domain. Z is set to be an RL circuit, therefore $Z = sL + R$, where s is the Laplace variable, L the shunt inductance and R the resistance.

Combining the three coupled equations, it is possible to obtain the out-of-plane compliance transfer function G:

$$G = \frac{W}{F} = \frac{1}{Ms^2 + Cs + K + 32\,\theta^2 \frac{s(sL+R)}{1+sC_p(sL+R)}} \tag{38}$$

where W and F are respectively the out-of-plane displacement of the end-effector and an external disturbance force expressed in the Laplace domain.

Subsequently, it is necessary to design the shunt circuits, i.e. the values for R and L need to be chosen. According to [11] there are two methods for choosing the "optimal" parameters for a RL-shunt circuit: the method based on transfer function considerations and the method based on pole placement considerations. The method of transfer

function considerations (which is analogue to the "equal-peak-design" presented in [6]) is used in this case, since it tends to give lower steady state responses compared to the other technique. Basically, the values for R and L are determined by the following formulae [11]:

$$R = \sqrt{2}\frac{K_i}{(1+{K_i}^2)C_p\omega_n} \tag{39}$$

$$L = \frac{1}{(1+{K_i}^2)C_p{\omega_n}^2} \tag{40}$$

where K_i is the effective electromechanical coupling factor, given by [12]:

$$K_i = \sqrt{\frac{32\ \theta^2}{KC_p}} \tag{41}$$

At this point, knowing also the geometrical and physical parameters of the structure, given in Table I and Table II, it is possible to determine and plot the out-of-plane compliance transfer function G.

The bode plot of the transfer function G is depicted in red in Figure 15. Furthermore, the situations where the piezoelectric patches are in open circuit and L-shunted are depicted. Overall, it can be observed that the attenuation at the resonance frequency is expected to be effective, about 15 dB, when using piezoelectric patches along to RL-shunt circuits. Furthermore, it can be noticed that the three plots do not intersect in a common point, like in Figure 6. This is caused by the influence of the material damping term C: if C was neglected, then the plots would intersect.

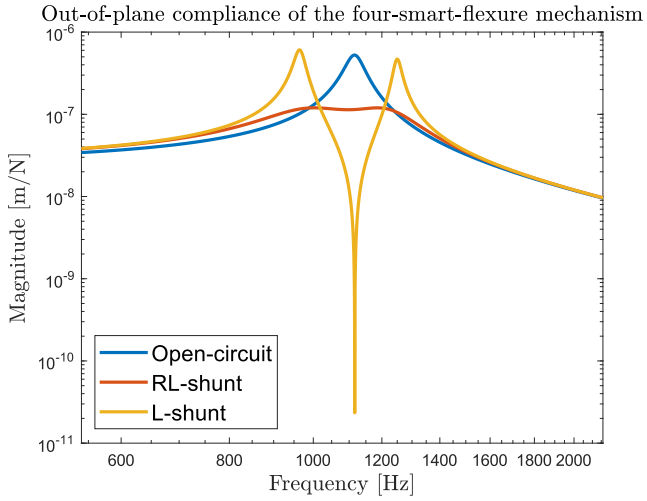

Fig. 15: Out-of-plane compliance of the four-smart-flexure mechanism with shunted piezoelectric patches

C. Addition of active control

As already mentioned, a passive technique such as piezoelectric shunt damping is recommended in the case of out-of-plane modes, since they are typically to be found at high frequencies, where active strategies can be detrimental for vibration attenuation due to spillover effects and bandwidth limitations. Nevertheless, it is worth trying to explore the possibility to add active control of the piezos next to the passive shunt circuits. In this case, the three coupled equations presented in the previous paragraph need to be adjusted, giving rise to the following system [17]:

$$(M_s+M_p)\ddot{w} + C\dot{w} + (K_s+K_p)w - 32\ \theta v_{piezo} = F \tag{42}$$

$$C_p\dot{v_{piezo}} + \theta\dot{w} = -\frac{v_{piezo}-v_{control}}{Z} = i \tag{43}$$

$$V_{piezo} + ZI = V_{control} \tag{44}$$

V_{piezo} indicates the voltage across each piezoelectric patch, in the Laplace domain, while $V_{control}$ indicates the control voltage.

It is worth noticing that in principle it is sufficient to have just one controller and one control voltage, given the fact that all the piezoelectric elements are characterized by the same capacitance C_p and the same coupling term $theta$. However, it is important to apply the control voltage in the right direction, i.e. on the right electrode: the different polarization direction between the patches, defined by ψ, gives the possibility to have all the electrodes on which to apply the control voltage on the same side.

Combining the three coupled equations, it is possible to obtain the following transfer function, which is identical to G except for the term involving $V_{control}$.

$$\frac{\dfrac{W}{F+32\ \theta\frac{V_{control}}{1+sC_p(sL+R)}}}{Ms^2+Cs+K+32\ \theta^2\frac{s(sL+R)}{1+sC_p(sL+R)}} = \frac{1}{} \tag{45}$$

Then, translating the aforementioned transfer function in a block diagram, the control structure would be the one depicted in Figure 16, defined by the following expressions:

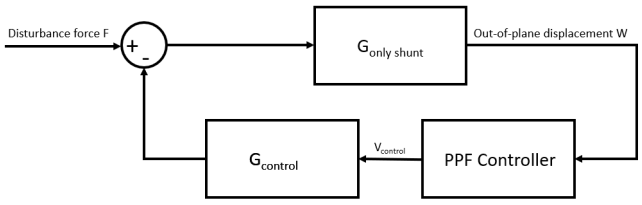

Fig. 16: Block diagram of the hybrid control structure

$$G_{control} = \frac{32\,\theta}{1 + sC_p(sL + R)} \tag{46}$$

$$G_{only\ shunt} = \frac{1}{Ms^2 + Cs + K + 32\,\theta^2 \frac{s(sL+R)}{1+sC_p(sL+R)}} \tag{47}$$

$$PPF = \frac{-g}{s^2 + 2\zeta_f\omega_f s + (w_f)^2} \tag{48}$$

The controller is chosen to be a Positive Position Feedback (PPF). Positive Position Feedback is one of the most attractive vibration control method due to its stability and ease of implementation. The transfer function PPF of such controller is given in Eq. (48).

Choosing the controller parameters as:
- $\omega_f = 1.7 \times \omega_s$
- $g = 5 \times 10^{14}$
- $\zeta_f = 0.7$

the closed-loop transfer function becomes the one depicted in Figure 17 and it can be noticed that the addition of active control can lead to higher performances. The term ω_s indicates the eigenfrequency of the structure when the shunt is in short circuit.

It can be noticed that in the block diagram of Figure 16 there is a term called $G_{control}$, besides the PPF controller and the passive plant $G_{only\ shunt}$, whose formulation is given in Eq. (47). This term reflects the amount of voltage that is actually going to contribute to give rise to a force opposing to the disturbance. Furthermore, it is worth noticing that $G_{control}$ represents a low-pass filter and above the electrical eigenfrequency of the shunt circuit the influence of the PPF controller is going to fade.

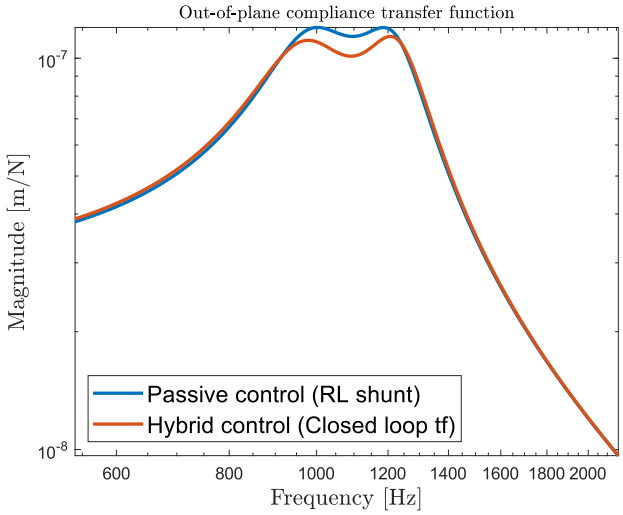

Fig. 17: Comparison of the out-of-plane compliance of the four-smart-flexure mechanism in the cases of hybrid and passive control

V. New mechanism to showcase the proposed principle of damping

As observed in the previous section, damping techniques based on piezoelectric materials represent an attractive solution for out-of-plane mode attenuation. Therefore, the goal of further research is to assess the effectiveness of the proposed design based on piezoelectric material with finite element methods.

In order to do so, it would be convenient to work on a modified and possibly simplified version of the mechanism proposed in Figure 14, since this mechanism is rather complex and, when excited, would mainly deform in the nominal direction of motion, while the interest of this work would be on out-of-plane deformations. In other words, the new set-up is designed to showcase the proposed principle of damping: once it is validated in this way, it is possible to proceed with experiments. This new version could be the one represented in Figure 18 and Figure 19, where the green elements represent the piezoelectric patches. This mechanism does not have any "compliant" degree of freedom, but the first eigenfrequency, depicted in Figure 20, represents an out-of-plane mode for the flexure in the middle, where the piezos are placed. The two other wider flexures are used as a guide and shaped in order to make the global stiffness in the z-direction higher than the global stiffness in the x-direction, so that the first eigenmode would occur along the x-direction which represents the out-of-plane direction for the flexure with the piezos.

The fact that the smart flexure in the middle is designed to be quite narrow is motivated by the fact that it is desired to have a relatively low eigenfrequency in order to ease future experiments on such mechanism. Indeed, a lower eigenfrequency of interest means that the excitation frequency and the sampling frequency used to identify the system can be lower. Furthermore, narrower flexures generally lead to more lightweight mechanism, which is a desired characteristic of future machines. Therefore, they are supposed to be used frequently and the study on their vibrations, including the out-of-plane modes, is of interest. Therefore, the final geometrical values, given in Table IV and Table III, are chosen with an eye on future experiments. In particular, they are chosen in order to fit the commercially available piezoelectric actuators of the BA series of Piezodrive [25].

At this point, having highlighted the kind of mechanism to be manufactured, the next experimental preliminary steps would be to redesign the shunt circuit, i.e. find the optimal value for the shunt impedance, and simulate the system numerically.

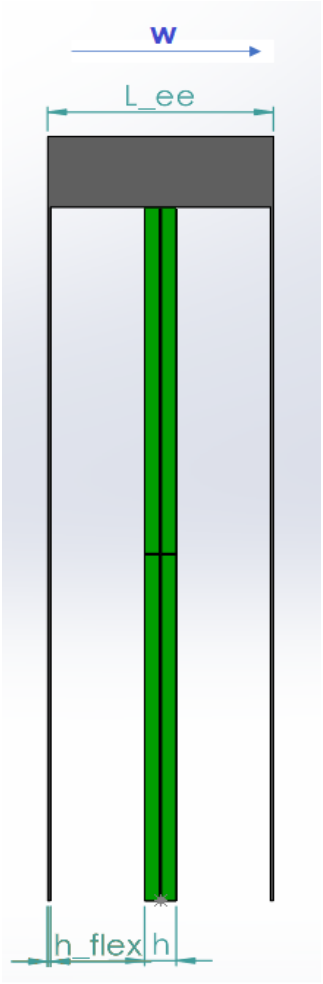

Fig. 18: Frontal view of the new version of flexure mechanism, specifically designed to test the vibration attenuation capabilities of piezoelectrics in the out-of-plane direction. The piezoelectric material is highlighted in green.

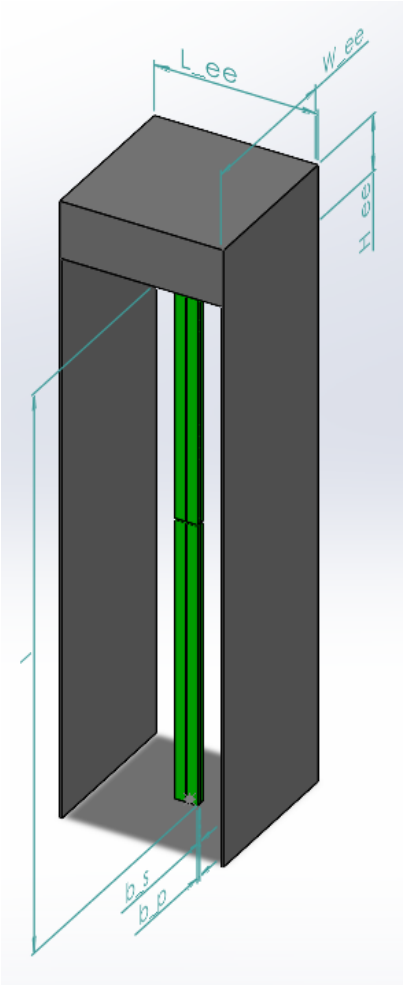

Fig. 19: 3D view of the new version of flexure mechanism

VI. Analytical and Finite Element Modeling of the New Mechanism

A. Analytical modeling

As discussed in the previous section, the mechanism of Figure 18 is now the object of study. The same procedure adopted to model the four-smart-flexure mechanism can also be applied to this new mechanism and the coupled equations of such system turn out to be the following:

$$(M_s + M_p)\ddot{w} + C\dot{w} + (K_s + K_p)w - 8\,\theta v = F \tag{49}$$

$$C_p\dot{v} + \theta\dot{w} = i \tag{50}$$

$$V = -ZI \tag{51}$$

where

$$\begin{aligned} M_s =& \rho_s h b_s \left(\frac{9l}{5} + \frac{4l}{7} - 2l\right) \\ &+ 2\rho_s h_{flex} Wee \left(\frac{9l}{5} + \frac{4l}{7} - 2l\right) \\ &+ \rho_s Wee H_{ee} L_{ee} \end{aligned} \tag{52}$$

$$M_p = 2\rho_p h b_p \left(\frac{9l}{5} + \frac{4l}{7} - 2l\right) \tag{53}$$

$$K_s = c_s b_s \frac{h^3}{l^3} + 2c_s W_{ee} \frac{h_{flex}^3}{l^3} \tag{54}$$

$$K_p = 2c_p b_p \frac{h^3}{l^3} \tag{55}$$

$$\theta = -\frac{3}{16l} d_{31} c_p h^2 \tag{56}$$

$$C_p = \epsilon_r \epsilon_0 \frac{hl}{4b_p} \tag{57}$$

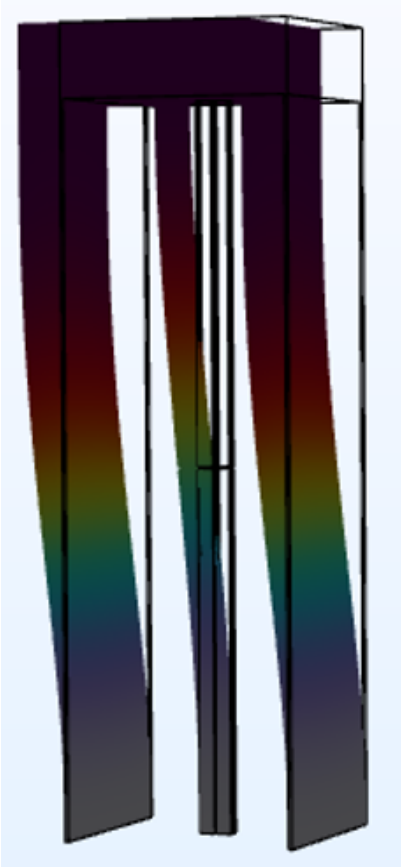

Fig. 20: First mode for the mechanism of Figure 19. It can be seen that the deformation of the flexure in the middle is of out-of-plane kind

Combining the three coupled equations, it is possible to obtain the out-of-plane compliance transfer function G:

$$G = \frac{W}{F} = \frac{1}{Ms^2 + Cs + K + 8\,\theta^2 \frac{s(sL+R)}{1+sC_p(sL+R)}} \tag{58}$$

where W and F are respectively the out-of-plane displacement of the end-effector and an external disturbance force, expressed in the Laplace domain.

The parameters used in the previous expressions are listed and described in Table III and Table IV.

Then, the RL shunt impedance can be designed according to Eq. (39) - Eq. (41), reported here for convenience:

$$R = \sqrt{2}\frac{K_i}{(1+{K_i}^2)C_p\omega_n} \tag{59}$$

$$L = \frac{1}{(1+{K_i}^2)C_p{\omega_n}^2} \tag{60}$$

where K_i is the effective electromechanical coupling factor, given by [12]:

$$K_i = \sqrt{\frac{8\,\theta^2}{KC_p}} \tag{61}$$

Parameter	Value	Unit	Description
b_p	0.0008	m	Piezoelectric patch width
c_s	68	GPa	Young's Modulus of the substrate
c_p	210	GPa	Young's Modulus of the piezos
ρ_s	7800	kg/m^3	Density of the substrate
ρ_p	7500	kg/m^3	Density of the piezos
ϵ_r	3130	/	Relative magnetic permeability
ϵ_0	$4\pi 10^{-7}$	$C^2/(Nm^2)$	Dielectric constant of vacuum
d_{31}	-274 10^{-7}	m/V	Coupling coefficient

TABLE III: Geometrical and physical parameters of the substrate structure of the new mechanisms of Figure 19, made of spring steel, and of the piezoelectric material, which is assumed to be PZT-5H

Parameter	Value	Unit	Description
h	0.0042	m	Height of the flexure substrate
b_s	0.0001	m	Width of the flexure substrate
l	0.0098	m	Lenght of the flexures
W_{ee}	0.08	m	Width pf the EE
L_{ee}	0.08	m	Lenght of the EE
H_{ee}	0.08	m	Height of the EE
h_{flex}	0.0004	m	Height of the guiding flexures

TABLE IV: Geometrical parameters of the system of Figure 19

B. Finite element modeling using COMSOL

At this point, knowing the geometrical and physical parameters of the substrate and the piezoelectric materials and the characteristics of the shunt circuit, it is possible to model the proposed mechanism in a finite element method (FEM) software. In particular, in this case the FEM program is $COMSOL\ Multiphysics$. In the case of piezoelectric materials, the physics of mechanics must be modelled together with the physics of electrostatics: therefore, the $Solid\ Mechanics$ and $Electrostatics$ physics are used within $COMSOL$. Furthermore, in order to model the shunt circuits, eight different $Electric\ circuits$ physics nodes are used to model the eight independent shunts. The results of the simulation are depicted in Figure 21, where a comparison with the results obtained analytically can be carried out.

The most noticeable difference between the FEM and analytical results is that $COMSOL$ shows that the attenuation is smaller than the one expected from Eq. (58): the attenuation predicted analytically is 17 dB, while $COMSOL$ shows that it only reaches 12 dB. This outcome is expected since the analytical model assumes that the strains are all of normal kind, since Euler-Bernoulli beam theory is adopted, whereas in a real case also shear stresses are present, especially in the case of relatively thick beams. Indeed, the out-of-plane deformations described in this work take place in the thick direction of the flexures and Euler-Bernoulli beam theory is more accurate in the case of slender beams. Timoshenko-beam theory is more accurate in the case of thick beams where shear stresses are dominant, but in this work it is decided to use Euler-Bernoulli beam theory since an eigenfrequency analysis of the mechanism

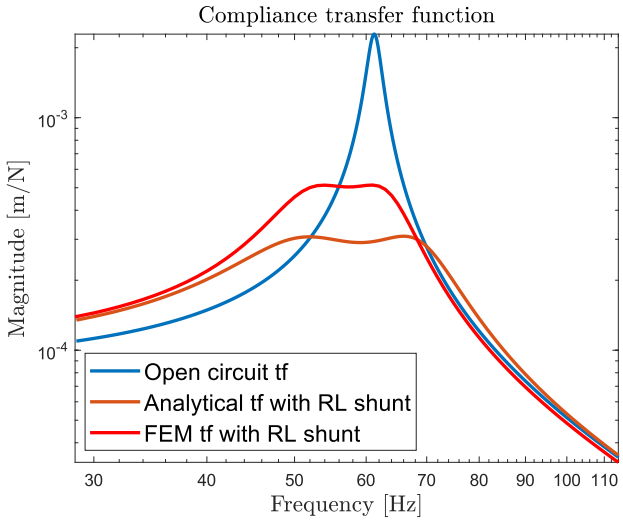

Fig. 21: Out of plane compliance transfer functions obtained with $COMSOL$ and analytically

of Figure 18 can show that at the first (out-of-plane) mode normal stresses are still dominant over the shear ones. Overall, the not negligible presence of shear stresses makes the analytical model relatively inaccurate but it represents a good first approximation. In particular, the reason why the vibration attenuation is not as high as expected analytically is the following: part of the strain is of shear instead of normal kind and, as a consequence, it is not coupled to the electrical domain by the d_{31} coefficient. Instead, it is coupled to it by the d_{24} coefficient, which is not relevant to add damping because such coupling does not give rise to charges where the electrodes are placed (the direction "3" in this case) but it produces charges on the surfaces along the direction "2". The 1-2-3 direction convention is represented in Figure 8 and the direction 3 typically indicates the direction in which the piezoelectric material is polarized.

Furthermore, in the $COMSOL$ model the values of the parameters for the shunt circuits are changed, i.e. they are not chosen to be the one calculated with Eq. (59) and Eq. (59). Indeed, such formulae hold in the case of pure bending. The new values are chosen through an iterative process, till the transfer function shows a satisfactory double-peak behavior. Even though the aforementioned expressions are not accurate anymore, they still give the right order of magnitude for the parameters of the shunt circuit: thus, finding the new optimal values for the shunt is not difficult.

Moreover, it can be observed that the double peak obtained from the $COMSOL$ simulation is slightly shifted towards lower frequencies. Again, this is expected since Euler-Bernoulli beam theory leads to overestimate the stiffness of beams by neglecting shear deformations and, as a consequence, overestimate also the eigenfrequency.

VII. Conclusion

In this paper, attention is drawn on the problem that out-of-plane modes could represent in flexure mechanisms. Then, a control strategy for out-of-plane vibrations in compliant systems is implemented, illustrated, both analytically and using FEM programs, and discussed. In particular, the focus is put on a passive solution, since out-of-plane modes are typically found at high frequencies. Furthermore, piezoelectric materials are used since they represent the most known and promising type of "smart material" and their passive implementation can lead to elegant and effective damping techniques. The results show that the proposed design is expected to provide satisfactory attenuation. Since the new concept is validated both analytically and in $COMSOL$, a recommendation for future work would be to conduct experimental tests in order to have a tangible proof of its effectiveness.

References

[1] "Compliant mechanisms explained." [Online]. Available: https://www.compliantmechanisms.byu.edu/about-compliant-mechanisms

[2] C. Vancura, I. Dufour, S. M. Heinrich, A. Hierlemann, and F. Josse, "Analysis of resonating microcantilevers operating in a viscous liquid environment," *Sensors and Actuators A Physical*, vol. A141, no. 1, pp. 43–51, 2008.

[3] B. J. Kenton and K. K. Leang, "Design and control of a three-axis serial-kinematic high-bandwidth nanopositioner," *IEEE/ASME Transactions on Mechatronics*, vol. 17, no. 2, pp. 356–369, 2012.

[4] K. K. Varanasi, S. A. Nayfeh, and A. H. Slocum, "Damping flexure mechanisms using low-density, low-wave-speed media," *ASME 2005 International Design Engineering Technical Conferences and Computers and Information in Engineering Conference*, 2005.

[5] K. Cai, Y. Tian, X. Liu, D. Zhang, J. Shang, and B. Shirinzadeh, "Development and control methodologies for 2-dof micro/nano positioning stage with high out-of-plane payload capacity," *Robotics and Computer-Integrated Manufacturing*, vol. 56, pp. 95–105, 2018.

[6] A. Preumont, *Vibration Control of Active Structures - An Introduction*, 4th ed., 2017, vol. 246.

[7] C. Vasques and J. D. Rodrigues, *Vibration and Structural Acoustics Analysis*, 2011.

[8] M. S. Weinberg, "Working equations for piezoelectric actuators and sensors," *JOURNAL OF MICROELECTROMECHANICAL SYSTEMS*, vol. 8, no. 4, pp. 529–533, 1999.

[9] L. Bin, L. Yugang, Y. Xuegang, and H. Shanglian, "Maximal modal force rule for optimal placement of point piezoelectric actuators for plates," *JOURNAL OF INTELLIGENT MATERIAL SYSTEMS AND STRUCTURES*, vol. 11, 2000.

[10] J. Gripp and D. Rade, "Vibration and noise control using shunted piezoelectric transducers: A review," *Mechanical Systems and Signal Processing*, vol. 112, pp. 359–383, 2018.

[11] N. W. Hagood and A. V. Flotow, "Damping of structural vibrations with piezoelectric materials and passive electrical networks," *Journal ofSound and Vibration*, vol. 146, no. 2, pp. 243–268, 1991.

[12] Y. Liao and H. Sodano, "Piezoelectric damping of resistively shunted beams and optimal parameters for maximum damping," *Journal of Vibration and Acoustics*, 2010.

[13] A. Bergamini, M. Zundel, and E. A. F. Parra, "Hybrid dispersive media with controllable wave propagation: A new take on smart materials," *Journal of Applied Physics*, vol. 118, no. 16, pp. 1–11, 2015.

[14] C. H. Park and A. Baz, "Vibration control of beams with negative capacitive shunting of interdigital electrode piezoceramics," *Journal of Vibration and Control*, vol. 11, pp. 331–346, 2005.

[15] D. Niederberger, A. Fleming, and M. Morari, "Adaptive multi-mode resonant piezoelectric shunt damping," *Smart Materials and Structures*, vol. 13, pp. 1025–1035, 2004.

[16] Y. Yang, Z. Jin, and C. KiongSoh, "Integrated optimal design of vibration control system for smart beams using genetic algorithms," *Journal of Sound and Vibration*, vol. 282, no. 3-5, pp. 1293–1307, 2005.

[17] J. Tang, K.-W. Wang, and M. Philen, "Sliding mode control of structural vibrations via active-passive hybrid piezoelectric networks," *Smart Structures and Materials*, 1999.

[18] M.S.Tsai and K.W.Wang, "On the structural damping characteristics of active piezoelectric actuators with passive shunt," *Journal of Sound and Vibration*, vol. 221, no. 1, pp. 1–22, 1999.

[19] H. F. L. dos Santos and M. A. Trindade, "Structural vibration control using extension and shear active-passive piezoelectric networks including sensitivity to electrical uncertainties," *Journal of the Brazilian Society of Mechanical Sciences and Engineering*, vol. 33, no. 3, pp. 287–301, 2011.

[20] B. Kim, W. W. Clark, and Q.-M. Wang, "Piezoelectric energy harvesting with a clamped circular plate: Analysis," 2014.

[21] Y. Liao and H. Sodano, "Model of a single mode energy harvester and properties for optimal power generation," *SMART MATERIALS AND STRUCTURES*, no. 17, 2008.

[22] C. D. Johnson, "Design of passive damping systems," *Journal of Mechanical Design*, vol. 117, no. B, pp. 171–176, 1995.

[23] B. Bandyopadhyay, T. Manjunath, and M. Umapathy, *Modeling, Control and Implementation of Smart Structures: A FEM-State Space Approach*, 2007.

[24] Z. Yanga, Y. Bai, and X. Chen, "Simultaneous optimal design of topology and size for a flexure-hinge-based guiding mechanism to minimize mass under stiffness and frequency constraints," *ENGINEERING OPTIMIZATION*, vol. 49, no. 6, pp. 948–961, 2017.

[25] "Piezodrive - piezo bender actuators." [Online]. Available: https://www.piezodrive.com/actuators/piezo-bender-actuators/

4

Mechanical design for out-of-plane mode attenuation in flexure mechanisms based on Eddy current damping

A potential solution to tackle out-of-plane modes is represented by Eddy current damping. Eddy current dampers (ECDs) are shown to provide effective attenuation for flexural modes [17] [26] [29]. Therefore, in this chapter it is determined whether ECDs are suitable also for out-of-plane vibration attenuation.

4.1. ECD-based mechanical design

A concept inspired by the designs of radial ECDs (an example of which is reported in Figure 4.1) is applied to the same four-flexure mechanism used in chapter 3, reported again in Figure 4.2 for convenience. The concept can be observed in Figure 4.3.

The end-effector is cut in order to give the possibility to place two repelling magnets in an effective way and, as a consequence, three different conductive layers, with thickness t, are present on the end-effector: one of them is between the magnets and sees a stronger radial magnetic field compared to the other two. Furthermore, some space is left between the magnets and the end-effector in the nominal direction of motion to allow its nominal movement. The distance between the conductive layers is indicated by d and w is the width of the conductive layers. Furthermore, the dimensions of the magnets in the x, y and z directions, according to the coordinate system of Figure 4.3, are are respectively $2a \times 2b \times 2c$ and the value of a,b and c are given in Table 4.1. When the structure moves in the out-of-plane direction, the conductive layers move perpendicularly to the radial magnetic flux, giving rise to ”circumferential” electromotive forces, which in turn create currents. It is worth noticing that the end-effector is supposed to be conductive only in selected regions (highlighted in red in Figure 4.3): indeed, if it was conductive everywhere, a damping action would occur also in the nominal direction of the flexure mechanism, which is undesired. Therefore, the end-effector is designed to be made of electrical conductive material only in the regions that see a relatively constant magnetic field when movement in the nominal direction occurs: if the magnetic flux concatenated by the conductive layers is constant, no damping action is observed in the nominal motion.

In order to find the damping coefficient c provided by the ECD, the following relation is used [17][26]:

$$c = \sigma \int_{V_c} {B_x}^2 + {B_y}^2 \, dV_c \tag{4.1}$$

where σ is the electrical conductivity of the conductive material, V_c is the volume of the conductive material, placed on the end-effector, and B_x and B_y are respectively the magnetic flux density in the x and y direction originated by the magnets: the sum of these two magnetic field intensities is equal to

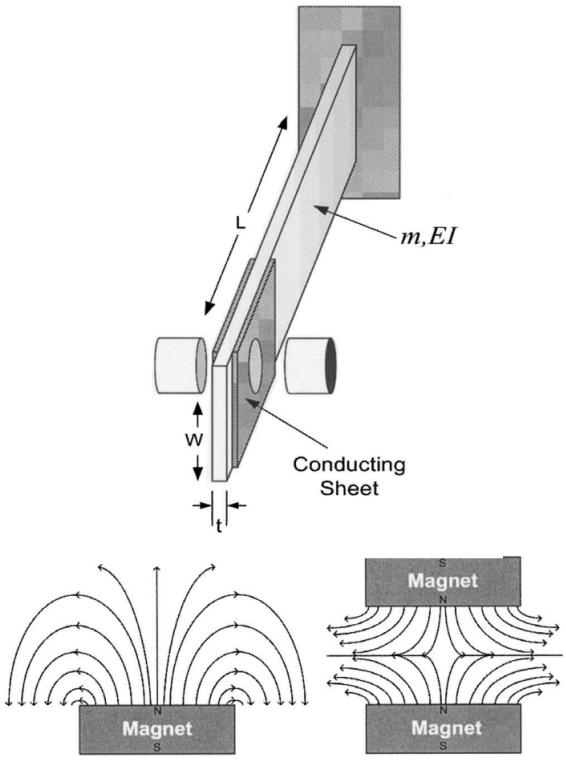

Figure 4.1: Radial Eddy current damper [26]. When the beam vibrates, the conductive plates located at its tip oscillate in the air gap between the magnets. Therefore, a conductive material moves in a magnetic field and, as a consequence, electric currents are generated, which in turn die out because of the resistance of the conductive plate, giving rise to a damping effect. In other words vibrational energy is converted into electric energy which dies out, providing a damping action. In particular, the magnetic field component that is relevant for the damping action is the ”radial” one, i.e. the one perpendicular to the axis connecting the two magnets: for this reason this kind of ECD is called ”radial”.

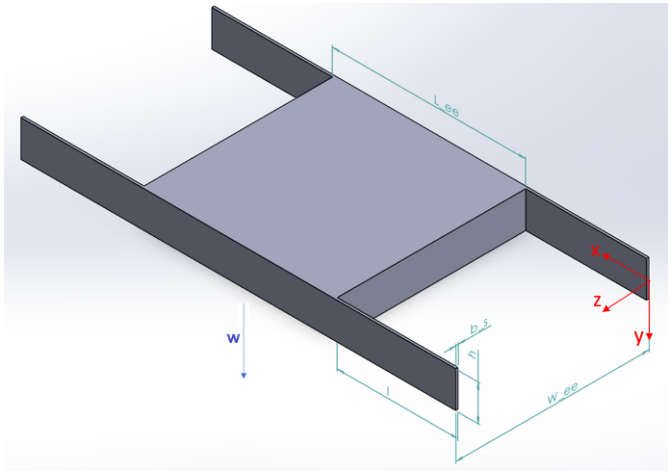

Figure 4.2: Typical 4-flexure mechanism whose out-of-plane vibrations need to be suppressed

the radial magnetic flux B_r. The integration is applied over the volume of the conductive material. It is worth noticing that the damping value given by the previous equation overestimates the real damping, cause it does not take into account the boundary conditions (that can be accounted for using the image method [30]) nor the skin-depth effect (whose modeling needs finite element softwares), but it already gives an acceptable first approximation, especially for low frequencies. Placing a local xyz coordinate system at the center of one of the cuboid magnets, as depicted in Figure 4.3, the formulation for the

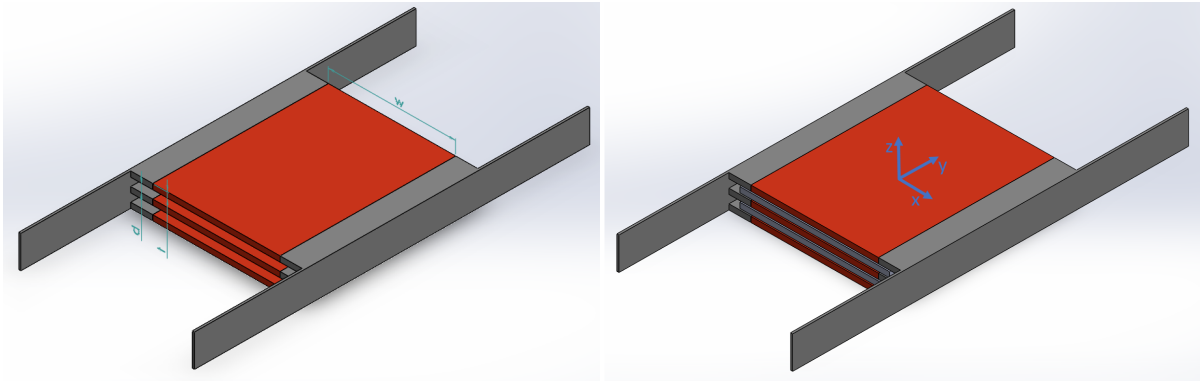

(a) (b)

Figure 4.3: Proposed concept of ECD to tackle out-of-plane modes of the mechanism of Figure 4.2. In (a) the layout of the modified end effector is reported, in (b) the repelling magnets are placed. The xyz coordinate system origin is located at the barycenter, i.e. the center of gravity, of the end-effector.

magnetic field in the x and y-direction that it produces is given by the following equations [31]:

$$B_x(x,y,z) = \frac{F_2(-x,y,-z)F_2(x,y,z)}{F_2(x,y,-z)F_2(-x,y,z)} \tag{4.2}$$

$$B_y(x,y,z) = \frac{F_2(-y,x,-z)F_2(y,x,z)}{F_2(y,x,-z)F_2(-y,x,z)} \tag{4.3}$$

where

$$F_2(x,y,z) = \frac{\sqrt{(x+a)^2+(y-b)^2+(z+c)^2}+b-y}{\sqrt{(x+a)^2+(y+b)^2+(z+c)^2}-b-y} \tag{4.4}$$

Parameter	Value	Unit
a	0.034	m
b	0.04	m
c	0.00125	m
d	0.00375	m
σ	5.96×10^7	S
t	0.0025	m
w	0.058	m

Table 4.1: Geometrical and physical properties of the proposed ECD design. The conductive material is assumed to be copper.

The total magnetic flux density is then obtained by the summation of the magnetic field produced by each magnet. Substituting the values of the parameters given in Table 4.1, it is possible to determine the damping coefficient for the particular case presented here. Furthermore, the equivalent stiffness matrix and mass matrices can be obtained using the same method used in the piezoelectric based solution presented in chapter 3. The damping coefficient is determined to be 4.4 Ns/m, which is too small to exert an effective damping action. Indeed, once the stiffness and mass matrices are known, it is possible to estimate the critical damping for this design and it turns out to be about 3000 Ns/m. Figure 4.4 depicts the out-of-plane compliance transfer function of the proposed system with radial ECD and it can be observed that the damping it provides is not satisfactory.

A possible way to improve the damping action is to ”split” the magnets in the y-direction, following the direction convention of Figure 4.3. Indeed, as can be noticed from Figure 4.5, the radial flux is maximum in correspondence of the projection of the edge of the magnet. The optimal number of ”splittings” would need to be determined by an optimization algorithm, since this splitting leads to have smaller

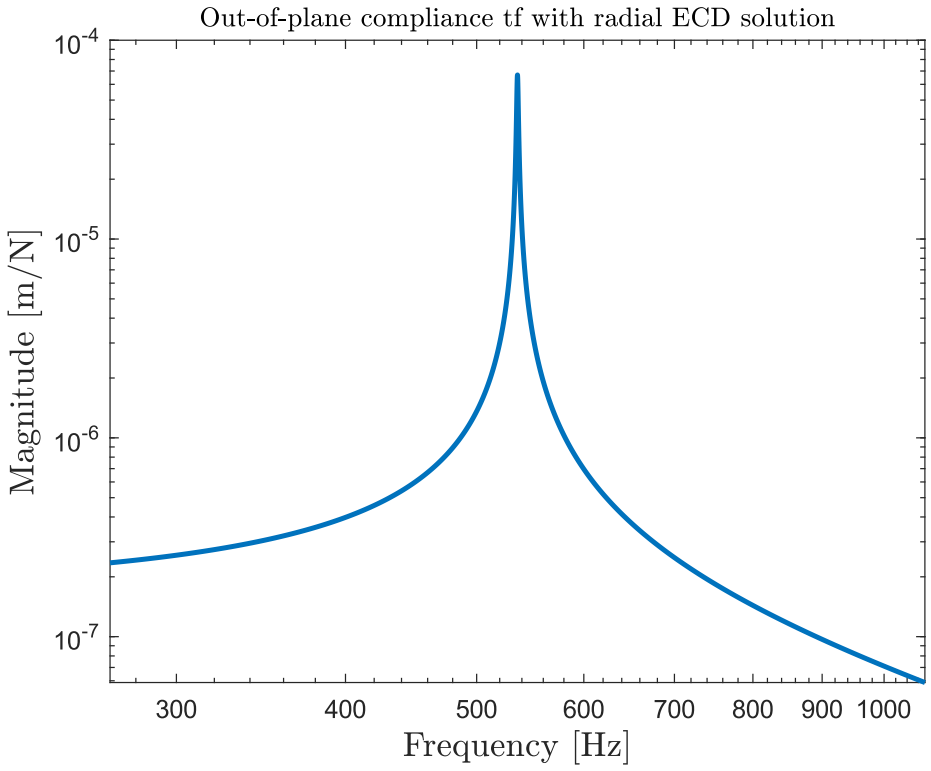

Figure 4.4: Out-of-plane compliance of the four-flexure mechanism using the proposed ECD

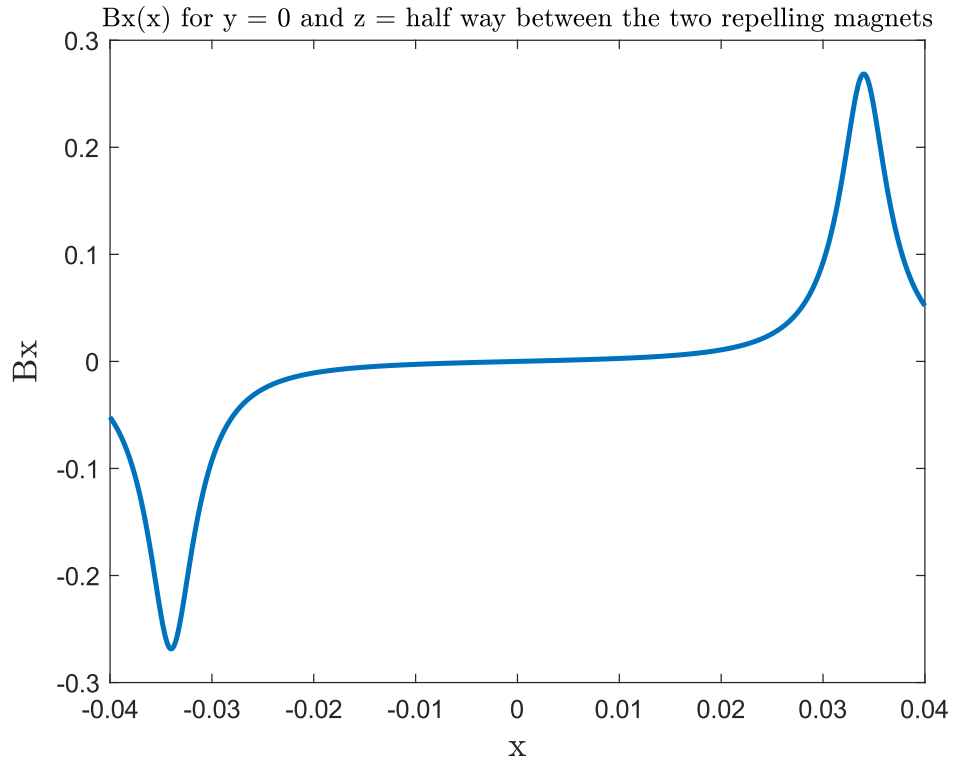

Figure 4.5: x-component of the magnetic field for fixed y,z coordinates

magnets and ”weaker” magnetic fields. These divisions can be done only in the y-direction since if it was done also in the x-direction, damping would occur also in the nominal direction of movement x, which has to be avoided. In any case, even though the design could be optimized, it is not expected to provide an acceptable amount of damping.

Alternatively, a completely different configuration relying on axial magnetic flux Eddy current dampers could be used. For example, the axial flux damper presented in [27] manages to provide a damping coefficient of about 2200 Ns/m, which in the case presented in the present work would be very effective. However, the damper of the cited paper is a lot bigger than the end-effector of Figure 4.2 (100 x 153 x 140 mm^3 vs 15 x 80 x 80 mm^3, therefore 22 times bigger) and its damping coefficient is proportional to the volume of the conductive material [27]. Thus, also this option does not look promising.

Other possible solutions involving magnets could be represented by magnetic negative stiffness dampers [24]. This kind of device consists in repelling magnets put both on the end-effector and on a outer stator, which would help to increase the out-of-plane stiffness. However, the equivalent stiffness provided by magnets is extremely low compared to the out-of-plane mechanical stiffness of typical flexure mechanism: therefore, this option is discarded. Another solution may be represented by ”magnetic” tuned mass dampers [32]: this solution, if applicable, would be very attractive since in this kind of TMD the non-linearity of the stiffness represented by the repelling magnets helps to attenuate the detuning problem, which is a common issue of classical TMDs. However, also in this case, the low stiffness provided by the magnets limits the applicability of this solution to the case presented here: indeed, the previously cited paper ([32]) applies the magnetic TMD to a large structure (an off-shore platform), whose natural frequency is very low compared to the one of flexure mechanisms in the out-of-plane direction.

In conclusion, Eddy current dampers and, more generally, vibration control solutions involving magnetic fields do not look promising to tackle the out-of-plane modes in flexure mechanisms, either because the damping action they provide is expected to be weak from analytical calculations or because of the low stiffness values that can be achieved using magnets. Furthermore, they are rather cumbersome and not compact devices.

5

Conclusion and Recommendations

5.1. Conclusion

In this thesis, the implementation of two new possible methods to tackle out-of-plane modes in flexure mechanisms is discussed. In particular, these two new alternatives are based on either piezoelectric materials or Eddy current dampers (ECDs).

On the one hand, the piezoelectric-based solution is demonstrated to be effective, both analytically and using FEM programs. However, the analytical model is not very accurate. Indeed, it is based on Euler-Bernoulli beam theory, which assumes that the strains in the flexure elements are entirely of normal kind, whereas in real deformations also shear strains are present, especially in the case of out-of-plane deflections. As a consequence, since a FEM software like $COMSOL\ Multiphysics$ is able to model also the shear nature of deformations, it gives much more accurate results. In particular, it is shown that the damping capability of the proposed design is not as high as it would be predicted analytically, but the attenuation is still very relevant. On the other hand, the ECD-based design turns out to be ineffective. Indeed, the amount of damping that ECDs can provide does not depend on the type of deformation, i.e. on the type of mode of vibration, differently from piezoelectric.based techniques. Therefore, the physical damping coefficient, expressed in Ns/m, that ECDs can provide is quite ”constant”. As a consequence, if ECDs are used for flexural mode attenuation, whose critical damping is relatively low, they represent a suitable damping option; if they are used for out-of-plane modes, whose critical damping is much higher (since the out-of-plane stiffness is much higher), they are not a favourable technique anymore.

Overall, the objective of this work to find a new damping technique able to deal with out-of-plane modes is accomplished. Furthermore, the previous solutions that can be found in the literature present drawbacks that are not present in the design proposed in this work. In particular, the piezoelectric-based solution adds very little mass to the system: moreover, considering a situation where piezoelectric patches are already present to tackle flexural modes, the weight addition is virtually absent. Furthermore, this damping method requires very little space, it can be applied in vacuum, it is not frequency dependent, it is stable and, if desired, it can easily become active, i.e. hybrid, differently from all the other previous techniques found in the literature.

5.2. Recommendations for future work

Even though the goal of the thesis is fulfilled, there is room for improvement. First, it would be worth testing the simplified concept proposed in chapter 3 in a real set-up. Secondly, it would be appropriate to develop its analytical model in order to account also for the shear stresses. In fact, this could give the possibility to design the shunt circuit using simple formulae without doing iterations in a FEM program. In other words, a possible future improvement of this work would be to update the formulae used to find the optimal RL-shunt impedance, which currently can hold only with the assumption of having an ideal Euler-Bernoulli beam. In fact, this assumption is acceptable when considering flexural deformations but not anymore when dealing with out-of-plane deflections.

Bibliography

[1] "Compliant mechanisms explained," [Online]. Available: https://www.compliantmechanisms.byu.edu/about-compliant-mechanisms.

[2] B. J. Kenton and K. K. Leang, "Design and control of a three-axis serial-kinematic high-bandwidth nanopositioner," *IEEE/ASME Transactions on Mechatronics*, vol. 17, no. 2, pp. 356–369, 2012. DOI: 10.1109/TMECH.2011.2105499.

[3] K. Cai, Y. Tian, X. Liu, D. Zhang, J. Shang, and B. Shirinzadeh, "Development and control methodologies for 2-dof micro/nano positioning stage with high out-of-plane payload capacity," *Robotics and Computer-Integrated Manufacturing*, vol. 56, pp. 95–105, 2018. DOI: 10.1016/j.rcim.2018.08.007.

[4] K. K. Varanasi, S. A. Nayfeh, and A. H. Slocum, "Damping flexure mechanisms using low-density, low-wave-speed media," *ASME 2005 International Design Engineering Technical Conferences and Computers and Information in Engineering Conference*, 2005. DOI: 10.1115/DETC2005-85448.

[5] A. Preumont, *Vibration Control of Active Structures - An Introduction*, 4th ed. 2017, vol. 246. DOI: 10.1007/978-3-319-72296-2.

[6] C. Vasques and J. D. Rodrigues, *Vibration and Structural Acoustics Analysis*. 2011. DOI: 10.1007/978-94-007-1703-9.

[7] M. S. Weinberg, "Working equations for piezoelectric actuators and sensors," *JOURNAL OF MICROELECTROMECHANICAL SYSTEMS*, vol. 8, no. 4, pp. 529–533, 1999. DOI: 10.1109/84.809069.

[8] L. Bin, L. Yugang, Y. Xuegang, and H. Shanglian, "Maximal modal force rule for optimal placement of point piezoelectric actuators for plates," *JOURNAL OF INTELLIGENT MATERIAL SYSTEMS AND STRUCTURES*, vol. 11, 2000. DOI: 10.1106/DE9J-B8Y5-1T4U-UM09.

[9] J. Gripp and D. Rade, "Vibration and noise control using shunted piezoelectric transducers: A review," *Mechanical Systems and Signal Processing*, vol. 112, pp. 359–383, 2018. DOI: 10.1016/j.ymssp.2018.04.041.

[10] N. W. Hagood and A. V. Flotow, "Damping of structural vibrations with piezoelectric materials and passive electrical networks," *Journal ofSound and Vibration*, vol. 146, no. 2, pp. 243–268, 1991. DOI: 10.1016/0022-460X(91)90762-9.

[11] Y. Liao and H. Sodano, "Piezoelectric damping of resistively shunted beams and optimal parameters for maximum damping," *Journal of Vibration and Acoustics*, 2010. DOI: 10.1115/1.4001505.

[12] A. Bergamini, M. Zundel, and E. A. F. Parra, "Hybrid dispersive media with controllable wave propagation: A new take on smart materials," *Journal of Applied Physics*, vol. 118, no. 16, pp. 1–11, 2015. DOI: 10.1063/1.4934202.

[13] C. H. Park and A. Baz, "Vibration control of beams with negative capacitive shunting of interdigital electrode piezoceramics," *Journal of Vibration and Control*, vol. 11, pp. 331–346, 2005. DOI: 10.1177/107754605040949.

[14] D. Niederberger, A. Fleming, and M. Morari, "Adaptive multi-mode resonant piezoelectric shunt damping," *Smart Materials and Structures*, vol. 13, pp. 1025–1035, 2004. DOI: 10.1088/0964-1726/13/5/007.

[15] Y. WU, L. LI, and Y. FAN, "A linearised analysis for structures with synchronized switch damping," *IEEE Access*, vol. 7, pp. 133 668–133 685, 2019, ISSN: 2169-3536 (ISSN). DOI: 10.1109/ACCESS.2019.2940823.

[16] S. Mohammadi, S. Hatam, and A. Khodayari, “Modeling of a hybrid semi-active/passive vibration control technique,” *Journal of Vibration and Control*, vol. 21, no. 1, pp. 21–28, 2015. DOI: 10.1177/1077546313479633.

[17] H. A. Sodano, J.-S. Bae, D. J. Inman, and W. K. Belvin, “Concept and model of eddy current damper for vibration suppression of a beam,” *Journal of Sound and Vibration*, vol. 288, no. 4-5, pp. 1177–1196, 2005. DOI: 10.1016/j.jsv.2005.01.016.

[18] H. F. L. dos Santos and M. A. Trindade, “Structural vibration control using extension and shear active-passive piezoelectric networks including sensitivity to electrical uncertainties,” *Journal of the Brazilian Society of Mechanical Sciences and Engineering*, vol. 33, no. 3, pp. 287–301, 2011. DOI: 10.1590/S1678-58782011000300004.

[19] Y. Yang, Z. Jin, and C. KiongSoh, “Integrated optimal design of vibration control system for smart beams using genetic algorithms,” *Journal of Sound and Vibration*, vol. 282, no. 3-5, pp. 1293–1307, 2005. DOI: 10.1016/j.jsv.2004.03.048.

[20] K. Chandrashekhara and A. Agarwal, “Active vibration control of laminated composite plates using piezoelectric devices: A finite element approach,” *Journal of Intelligent Material Systems and Structures*, vol. 4, pp. 496–508, 1993. DOI: 10.1177/1045389X9300400409.

[21] J. B. LISELI, J. AGNUS, and P. LUTZ, “An overview of piezoelectric self-sensing actuation for nanopositioning applications: Electrical circuits, displacement and force estimation,” *IEEE Transactions on Instrumentation and Measurement*, 2019. DOI: 10.1109/TIM.2019.2950760.

[22] J. Tang, K.-W. Wang, and M. Philen, “Sliding mode control of structural vibrations via active-passive hybrid piezoelectric networks,” *Smart Structures and Materials*, 1999. DOI: 10.1117/12.350732.

[23] M.S.Tsai and K.W.Wang, “On the structural damping characteristics of active piezoelectric actuators with passive shunt,” *Journal of Sound and Vibration*, vol. 221, no. 1, pp. 1–22, 1999. DOI: 10.1006/jsvi.1998.1841.

[24] E. Diez-Jimenez, R. Rizzo, M.-J. Gomez-Garcia, and E. Corral-Abad, “Review of passive electromagnetic devices for vibration damping and isolation,” *Hindawi, Shock and Vibration*, vol. 2019, 2019. DOI: 10.1155/2019/1250707.

[25] Z. W. Huang, X. G. Hua, Z. Q. Chen, and H. W. Niu, “Modeling, testing, and validation of an eddy current damper for structural vibration control,” *Journal of Aerospace Engineering*, vol. 31, no. 5, 2018. DOI: 10.1061/(ASCE)AS.1943-5525.0000891.

[26] H. A. Sodano, J.-S. Bae, and D. J. Inman, “Improved concept and model of eddy current damper,” *Journal of Vibration and Acoustics*, vol. 128, no. 3, pp. 294–302, 2006. DOI: 10.1115/1.2172256.

[27] L. Zuo, X. Chen, and S. Nayfeh, “Design and analysis of a new type of electromagnetic damper with increased energy density,” *Journal of Vibration and Acoustics*, vol. 133, no. 041006, 2011. DOI: 10.1016/j.mechatronics.2012.08.002.

[28] I. Valiente-Blanco, C. Cristache, J. Sanchez-Garcia-Casarrubios, F. Rodriguez-Celis, and J.-L. Perez-Diaz, “Mechanical impedance matching using a magnetic linear gear,” *Hindawi, Shock and Vibration*, vol. 2017, 2017. DOI: 10.1155/2017/7679390.

[29] H. A. Sodano and D. J. Inman, “Modeling of a new active eddy current vibration control system,” *Journal of Dynamic Systems, Measurement and Control*, vol. 130, no. 021009, pp. 1–11, 2011. DOI: DOI:10.1115/1.2837436.

[30] H. A. Sodano and J.-S. Bae, “Eddy current damping in structures,” *The Shock and Vibration Digest*, vol. 36, no. 6, pp. 469–478, 2005. DOI: 10.1177/0583102404048517.

[31] J. M. Camacho and V. Sosa, “Alternative method to calculate the magnetic field of permanent magnets with azimuthal symmetry,” *Revista Mexicana de Fisica E*, vol. 59, no. 1, pp. 8–17, 2013. [Online]. Available: https://www.researchgate.net/publication/262707508_Alternative_method_to_calculate_the_magnetic_field_of_permanent_magnets_with_azimuthal_symmetry.

[32] Q. Wu, W. Zhao, and W. Zhu, “A tuned mass damper with nonlinear magnetic force for vibration suppression with wide frequency range of offshore platform under earthquake loads,” *Hindawi - Shock and Vibration*, vol. 2018, 2018. DOI: 10.1155/2018/1505061.

A

Matlab code for the piezoelectric-based design - Part 1

A.1. Design for the four-flexure mechanism

In this section, the MATLAB code used to model the piezoelectric-based solution applied on the four-flexure mechanism of chapter 3 is reported.

```
clc
clear all
close all

set(0,'defaulttextinterpreter','Latex');

s = tf('s');

b_s = 0.001; %m
b_p = 0.001; %m
h = 0.015; %m
l = 0.05; %m
H_ee = 0.08; %m
L_ee = 0.08; %m

c_s = 210*10^9; %Pa Steel
c_p = 60*10^9; %Pa PZT-5H
d31 = -274*10^(-12); %m/V

I_s = b_s*h^3/12;
I_p = 2*b_p*h^3/12;

K_s = c_s*b_s*h^3/l^3;
K_p = 2*c_p*b_p*h^3/l^3;

K = 4 * (K_s + K_p);

rho_s = 7800; %kg/m^3
rho_p = 7500;
M_s = rho_s*h*b_s*(9*l/5+4*l/7-2*l);
M_p = 2*rho_p*h*b_p*(9*l/5+4*l/7-2*l);
M = 4 * (M_s + M_p) + rho_s*(h*H_ee*L_ee);

theta = -3/8*d31*c_p*h^(2)/(2*l);
```

```
epsilon_r = 1500;
epsilon_0 = 8.9 * 10^(-12);
Cp = epsilon_r*epsilon_0*(h/2)*(l/2)/b_p;

Ki = ((theta*sqrt(32))^2/(Cp*K))^0.5;

ws = (K/M)^0.5;
w0 = (ws^2 + theta^2/(M*Cp))^0.5;

wn = ws*1.00;

R = (2)^(0.5) * Ki/((1+Ki^2)*Cp*wn); %Hagood
L = 1/((1+Ki^2)*Cp*(wn)^2); %Hagood

C = 0.02*2*sqrt(K/M);

G_SC = 1/(M*s^2 + C*s + K);
G1 = 1/(M*s^2 + C*s + K + 32*theta^2/Cp);
G2 = 1/(M*s^2 + C*s + K + 32*theta^2 * (s*(s*L+R)/(1+s*Cp*(s*L+R))));
G3 = 1/(M*s^2 + C*s + K + 32*theta^2 * (s*(s*L)/(1+s*Cp*(s*L))));

[mag1,phase1,wout1] = bode(G1,linspace(wn/2,wn*2,10000));
Wout1 = (wout1(:))/(2*pi);
Mag1=(mag1(:)); Phase1=phase1(:);
figure(1);
loglog(Wout1,Mag1,'LineWidth',2);
hold on
[mag2,phase2,wout2] = bode(G2,linspace(wn/2,wn*2,10000));
Wout2 = (wout2(:))/(2*pi);
Mag2=(mag2(:)); Phase2=phase2(:);
loglog(Wout2,Mag2,'LineWidth',2);
hold on
[mag3,phase3,wout3] = bode(G3,linspace(wn/2,wn*2,10000));
Wout3 = (wout3(:))/(2*pi);
Mag3=(mag3(:)); Phase3=phase3(:);
loglog(Wout3,Mag3,'LineWidth',2);
hold on
title = title('Out-of-plane compliance of the four-smart-flexure mechanism');
title.FontSize = 14;
hold on
y = ylabel('Magnitude [m/N]');
y.FontSize = 14;
x = xlabel('Frequency [Hz]');
x.FontSize = 14;
lgd = legend('Open-circuit','RL-shunt','L-shunt');
lgd.FontSize = 14;

G_control = 32*theta/(1+s*Cp*(R+s*L));

L2 = L*1;
R2 = R*1;
G_only_shunt = 1/(M*s^2 + C*s + K + 32*theta^2 * (s*(s*L2+R2)/(1+s*Cp*(s*L2+R2))));

wf = 5*ws;
g = 10*10^14;
```

```
Cf = 0.7;
PPF = -g/(s^2 + 2*Cf*wf*s + wf^2);


CL_PPF = G_only_shunt / (1 + G_only_shunt*G_control*PPF);
pole(CL_PPF)

figure(2)
[mag2,phase2,wout2] = bode(G2,linspace(wn/2,wn*2,10000));
Wout2 = (wout2(:))/(2*pi);
Mag2=(mag2(:)); Phase2=phase2(:);
loglog(Wout2,Mag2,'LineWidth',2);
hold on
[mag4,phase4,wout4] = bode(CL_PPF,linspace(wn/2,wn*2,10000));
Wout4 = (wout4(:))/(2*pi);
Mag4=(mag4(:)); Phase4=phase4(:);
loglog(Wout4,Mag4,'LineWidth',2);
hold on
%title = title('Compliance transfer function');
%title.FontSize = 14;
hold on
y = ylabel('Magnitude [m/N]');
y.FontSize = 14;
x = xlabel('Frequency [Hz]');
x.FontSize = 14;
lgd = legend('Hybrid control (Closed loop tf)','Passive control (RL shunt)');
lgd.FontSize = 14;
```

B

Matlab code for the piezoelectric-based design - Part 2

B.1. Design for the new mechanism

In this section, the MATLAB code used to model the piezoelectric-based solution applied on the new simplified mechanism of chapter 3 is reported.

```
clc
clear all
close all

set(0,'defaulttextinterpreter','Latex');

s = tf('s');

b_s = 0.0001; % m
b_p = 0.0008; % m
h = 0.0042; % m
h_p = 0.0021; % m
l = 0.098; % m
l_p = 0.049; % m
L_ee = 0.03; % m
W_ee = 0.03; % m
H_ee = 0.01; % m
b_flex = W_ee;
h_flex = 0.0004; % m

c_p = 61.1 * 10^9; % PZT5H
c_s = 210 * 10^9; % Spring steel

d31 = -274*10^(-12); % m/V

I_s = b_s*h^3/12;
I_p = 2*b_p*h^3/12;

K_s = c_s*b_s*h^3/l^3;
K_p = 2*c_p*b_p*h^3/l^3;

I_flex = b_flex*h_flex^3/12;
K_flex = 2*c_s*b_flex*h_flex^3/l^3;
```

```
K = K_s + K_p + K_flex;

rho_s = 7800; %kg/m^3
rho_p = 7500; %kg/m^3
M_s = rho_s*h*b_s*(9*l/5+4*l/7-2*l);
M_p = 2*rho_p*h*b_p*(9*l/5+4*l/7-2*l);
M_flex = 2*rho_s*h_flex*b_flex*(9*l/5+4*l/7-2*l);
M_ee = rho_s*(L_ee*W_ee*H_ee);
M = (M_s + M_p + M_flex) + M_ee;

theta = -3/8*d31*c_p*h^(2)/(2*l);

epsilon_r = 1500;
epsilon_0 = 8.8541878128 * 10^(-12);
Cp = epsilon_r*epsilon_0*(h/2)*(l/2)/b_p;

Ki = ((theta*sqrt(8))^2/(Cp*K))^0.5;

ws = (K/M)^0.5;
w0 = (ws^2 + theta^2/(M*Cp))^0.5;
wn = ws*1.003;
fn = wn/(2*pi);
R = (2)^(0.5) * Ki/((1+Ki^2)*Cp*wn); %Hagood
L = 1/((1+Ki^2)*Cp*(wn)^2); %Hagood

C = 0.02 * 2*sqrt(K*M);
C_crit = 2*sqrt(K*M);

G1 = 1/(M*s^2 + C*s + K + 8*theta^2/Cp);
G2 = 1/(M*s^2 + C*s + K + 8*theta^2 * (s*(s*L+R)/(1+s*Cp*(s*L+R))));
G3 = 1/(M*s^2 + C*s + K + 8*theta^2 * (s*(s*L)/(1+s*Cp*(s*L))));

bode(G1,G2)

%return

G_control = 8*theta/(1+s*Cp*(R+s*L));

L2 = L*0.8;
R2 = R*1;
G_only_shunt = 1/(M*s^2 + C*s + K + 8*theta^2 * (s*(s*L2+R2)/(1+s*Cp*(s*L2+R2))));
wf = 2*ws;
g = 10*10^10;
Cf = 0.55;
PPF = -g/(s^2 + 2*Cf*wf*s + wf^2);

CL_PPF = G_only_shunt / (1 + G_only_shunt*G_control*PPF);
pole(CL_PPF)
bode(CL_PPF,G2)

COMSOL = readmatrix('COMSOL_tf_aug_1.txt');
f_vector = COMSOL(:,1);
compliance_vector = COMSOL(:,2);

COMSOL_OC = readmatrix('COMSOL_tf_aug_1_OC.txt');
f_vector_OC = COMSOL_OC(:,1);
```

```
compliance_vector_OC = COMSOL_OC(:,2);

[mag1,phase1,wout1] = bode(G1,linspace(wn/2,wn*2,10000));
Wout1 = (wout1(:))/(2*pi);
Mag1=(mag1(:)); Phase1=phase1(:);
figure;
loglog(Wout1,Mag1,'LineWidth',2);
xlim([28.6 114])
hold on
[mag,phase,wout] = bode(G2,linspace(wn/2,wn*2,10000));
Wout = (wout(:))/(2*pi);
Mag=(mag(:)); Phase=phase(:);
loglog(Wout,Mag,'LineWidth',2);
hold on
plot(f_vector,compliance_vector,'r','LineWidth',2.0)
hold on
%plot(f_vector_OC,compliance_vector_OC,'y','LineWidth',2.0)
%hold on
lgd = legend('Open circuit tf','Analytical tf with RL shunt','FEM tf with RL shunt');
lgd.FontSize = 14;
hold on
title = title('Compliance transfer function');
title.FontSize = 14;
hold on
y = ylabel('Magnitude [m/N]');
y.FontSize = 14;
x = xlabel('Frequency [Hz]');
x.FontSize = 14;
```

C

Matlab code for the ECD-based design

C.1. Design for the four-flexure mechanism

In this appendix, the MATLAB code used to model the ECD-based solution applied on the four-flexure mechanism of Figure 4.2 is reported.

```
clc
clear all
close all

set(0,'defaulttextinterpreter','Latex');

u0 = 4*pi*10^(-7);
Br = 1;
M = Br/u0;

a = 0.034;
b = 0.04;
c = 0.00125;

d = 0.00375;

sigma = 5.96*10^7;

syms x y
syms z

z2 = z - d - 2*c;

F2 = (sqrt((x+a)^2+(y-b)^2+(z+c)^2) + b - ...
    y)/(sqrt((x+a)^2+(y+b)^2+(z+c)^2) - b - y);

Bx_1 = u0*M/(4*pi)*log(subs(F2,[x,y,z],[-x,y,...
    -z]) * F2 / (subs(F2,[x,y,z],[x,y,...
    -z])* subs(F2,[x,y,z],[-x,y,z])));
By_1 = u0*M/(4*pi)*log(subs(F2,[x,y,z],[-y,x,...
    -z]) * subs(F2,[x,y,z],[y,x,...
    z]) / (subs(F2,[x,y,z],[y,x,...
    -z])*subs(F2,[x,y,z],[-y,x,z])));

Bx_2 = subs(-u0*M/(4*pi)*log(subs(F2,[x,y,...
    z],[-x,y,-z]) * F2 / (subs(F2,[x,y,...
```

```
    z],[x,y,-z]) * subs(F2,[x,y,z],[-x,y,...
    z])),z,z2);
By_2 = subs(-u0*M/(4*pi)*log(subs(F2,[x,y,...
    z],[-y,x,-z]) * subs(F2,[x,y,z],[y,x,...
    z]) / (subs(F2,[x,y,z],[y,x,...
    -z]) * subs(F2,[x,y,z],[-y,x,z]))),z,z2);

Bx = Bx_1 + Bx_2;
By = By_1 + By_2;

Bx_x = subs(Bx,[y z],[0 0.0025+0.000625]);
n = 500;
x_ar = linspace(-0.04,0.04,n);
coun = 1;
Bx_x_ar = zeros(1,n);
for coun=1:n
    Bx_x_ar(coun) = subs(Bx_x,x,x_ar(coun));
end
plot(x_ar,Bx_x_ar,'Linewidth',2)
title('Bx(x) for y = 0 and z = half way between the two repelling magnets')
xlabel('x')
ylabel('Bx')

n = 20;
x_min = -0.029;
x_max = x_min*(-1);
x_array = linspace(x_min,x_max,n);
f = 0;
counter = 2;

for (counter = 2:n)
df(counter) = (x_max-x_min)/n*(((subs((Bx^2 + By^2),x,x_array(counter))+...
    subs((Bx^2+By^2),x,x_array(counter-1)))))/2;
f = f + df(counter);
end

counter = 2;
n = 20;
y_min = -0.040;
y_max = y_min*(-1);
y_array = linspace(y_min,y_max,n);
g = 0;

for (counter = 2:n)
dg(counter) = (y_max-y_min)/n*(((subs(f,y,...
    y_array(counter))+subs(f,y,...
    y_array(counter-1)))))/2;
g = g + dg(counter);
end

counter = 2;
n = 20;
z_min = 0.001875;
z_max = 0.004375;
z_array = linspace(z_min,z_max,n);
h = 0;
```

```
for (counter = 2:n)
dh(counter) = (z_max-z_min)/n*((subs(g,z,...
    z_array(counter))+subs(g,z,...
    z_array(counter-1))))/2;
h = h + dh(counter);
end
h = vpa(h);
c_damping = h*sigma;
```